Oxylipin biosynthesis reinforces cellular senescence and allows detection of senolysis

Wiley, Christopher D; Sharma, Rishi; Davis, Sonnet S; Lopez-Dominguez, Jose Alberto; Mitchell, Kylie P; Wiley, Samantha; Alimirah, Fatouma; Kim, Dong Eun; Payne, Therese; Rosko, Andrew

Published in:
Cell metabolism

DOI:
10.1016/j.cmet.2021.03.008

Document Version
Publisher's PDF, also known as Version of record

Publication date:
2021

Cell Metabolism

Article

Oxylipin biosynthesis reinforces cellular senescence and allows detection of senolysis

Graphical abstract

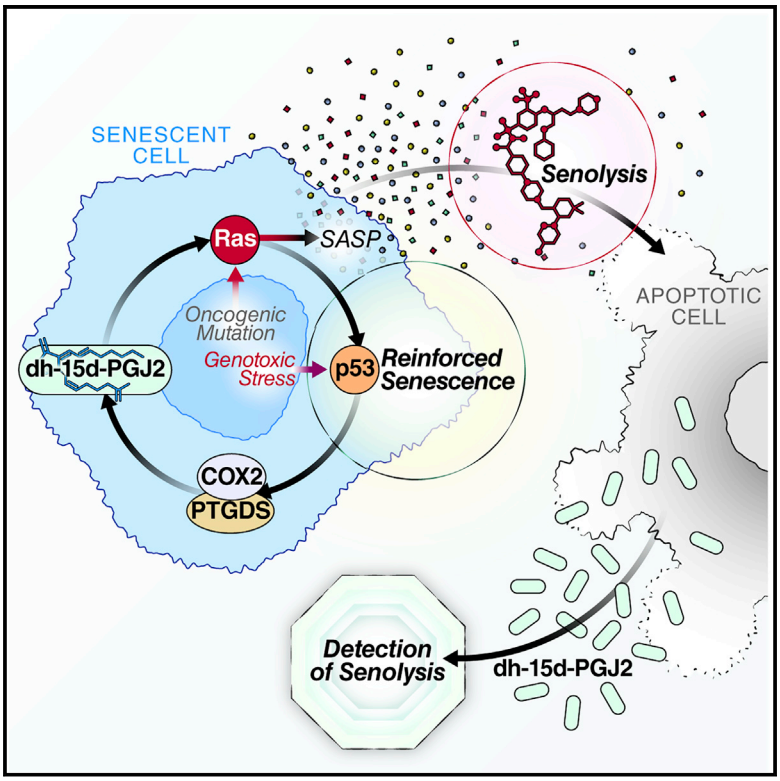

Highlights

- Senescent cells make several oxylipins, dihomo-prostaglandins, and leukotrienes
- Dihomo-15d-PGJ2 is intracellular during senescence and released during senolysis
- Dihomo-15d-PGJ2 activates RAS, promoting senescence and the SASP
- Positive feedback between prostaglandins, RAS, and p53 maintains senescence

Authors

Christopher D. Wiley, Rishi Sharma, Sonnet S. Davis, ..., Marco Demaria, Arvind Ramanathan, Judith Campisi

Correspondence

christopher.wiley@tufts.edu (C.D.W.), arvind@instem.res.in (A.R.), jcampisi@buckinstitute.org (J.C.)

In brief

Senolytics, transgenic, and pharmacological interventions that selectively kill senescent cells are currently in clinical trials aiming to treat age-related degenerative pathologies. Here, Wiley et al. discover that senescent cells produce multiple signaling lipids known as oxylipins. One oxylipin, dihomo-15d-PGJ2, promotes features of senescence by activating RAS and is released from cells during senolysis, serving as the first biomarker of the process in culture and *in vivo*.

Wiley et al., 2021, Cell Metabolism *33*, 1124–1136
June 1, 2021
https://doi.org/10.1016/j.cmet.2021.03.008

CellPress

CellPress

Cell Metabolism

Article

Oxylipin biosynthesis reinforces cellular senescence and allows detection of senolysis

Christopher D. Wiley,[1,2,*] Rishi Sharma,[1] Sonnet S. Davis,[1] Jose Alberto Lopez-Dominguez,[1] Kylie P. Mitchell,[1] Samantha Wiley,[1] Fatouma Alimirah,[1] Dong Eun Kim,[1] Therese Payne,[1] Andrew Rosko,[1] Eliezer Aimontche,[1] Sharvari M. Deshpande,[1] Francesco Neri,[1] Chisaka Kuehnemann,[1] Marco Demaria,[1,3] Arvind Ramanathan,[1,4,*] and Judith Campisi[1,5,6,*]

[1]Buck Institute for Research on Aging, 8001 Redwood Boulevard, Novato, CA 94945, USA

[2]Jean Mayer USDA Human Nutrition Research Center on Aging at Tufts University, Boston, MA 02111, USA

[3]European Research Institute for the Biology of Aging (ERIBA), University Medical Center Groningen (UMCG), Antonius Deusinglaan 1, 9713 Groningen, the Netherlands

[4]Institute for Stem Cell Science and Regenerative Medicine, GKVK - Post, Bellary Road, Bengaluru, Karnataka 560065, India

[5]Lawrence Berkeley National Laboratory, 1 Cyclotron Road, Berkeley, CA 94720, USA

[6]Lead contact

*Correspondence: christopher.wiley@tufts.edu (C.D.W.), arvind@instem.res.in (A.R.), jcampisi@buckinstitute.org (J.C.)

https://doi.org/10.1016/j.cmet.2021.03.008

SUMMARY

Cellular senescence is a stress or damage response that causes a permanent proliferative arrest and secretion of numerous factors with potent biological activities. This senescence-associated secretory phenotype (SASP) has been characterized largely for secreted proteins that participate in embryogenesis, wound healing, inflammation, and many age-related pathologies. By contrast, lipid components of the SASP are understudied. We show that senescent cells activate the biosynthesis of several oxylipins that promote segments of the SASP and reinforce the proliferative arrest. Notably, senescent cells synthesize and accumulate an understudied intracellular prostaglandin, 1a,1b-dihomo-15-deoxy-delta-12,14-prostaglandin J2. Released 15-deoxy-delta-12,14-prostaglandin J2 is a biomarker of senolysis in culture and *in vivo*. This and other prostaglandin D2-related lipids promote the senescence arrest and SASP by activating RAS signaling. These data identify an important aspect of cellular senescence and a method to detect senolysis.

INTRODUCTION

Cellular senescence is a multifaceted response to physiological and stress-generated signals, resulting in an essentially permanent arrest of cell proliferation and several phenotypic changes, including cellular hypertrophy, nuclear and epigenetic rearrangements, and metabolic alterations (Kuilman et al., 2010; Wiley and Campisi, 2016). Cell culture and transgenic mouse studies show that senescent cells can drive several age-associated pathologies in part by secreting a myriad of biologically active molecules. These molecules, which include inflammatory cytokines and chemokines, proteases, and growth factors, can have potent local—and potentially systemic—effects on tissues (Acosta et al., 2008; Coppé et al., 2008). Senescent cells increase with age in human and mouse tissues (Campisi, 2013; Wiley and Campisi, 2016), which, at least in mice, limits both median lifespan and healthspan (Baker et al., 2016).

Thus far, the senescence-associated secretory phenotype (SASP) has been studied primarily with regard to secreted proteins (Coppé et al., 2008; Wiley et al., 2019b). Here, we show that senescent cells also synthesize a number of oxylipins, which are a class of biologically active lipids that arise from the oxygenation of polyunsaturated fatty acids (PUFAs). Oxylipins have diverse physiological effects, including inflammation, fever, vasoconstriction and vasodilation, pain, hair loss, asthma, and fibrosis (Funk, 2001; Soberman and Christmas, 2003). Senescent cells are known to produce prostaglandin E2 (PGE2) (Cormenier et al., 2018; Dagouassat et al., 2013; Kabir et al., 2016; Martien et al., 2013; Yang et al., 2011; Zdanov et al., 2007), and the leukotriene-producing 5-lipoxygenase activity was shown to increase in replicative and oncogene-induced senescence, where it reinforced senescence-associated phenotypes by increasing reactive oxygen species (Catalano et al., 2005). We show that senescent human cells synthesize a much larger set of oxylipins, including PGD2 and its derivatives, 22-carbon PUFAs and monounsaturated fatty acids (MUFAs). Further, the dihomo-prostaglandins, less-studied derivatives of adrenic acid, are the primary prostaglandins produced by senescent cells, and one of these derivatives, dihomo-15d-PGJ2, is an intracellular biomarker of senescence and its release from cells is a hallmark of senolysis in culture and *in vivo*.

RESULTS

Cellular senescence activates oxylipin biosynthesis

The senescence arrest and SASP entail significant changes in metabolism (Wiley and Campisi, 2016), including lipid metabolism (Buratta et al., 2017; Cadenas et al., 2012; Catalano

et al., 2005; Flor et al., 2017; Quijano et al., 2012). To better understand these changes, we extracted intracellular lipids from cultured human fibroblasts (IMR-90) that were either proliferating (PRO, 10% serum), quiescent (QUI, 0.2% serum), or induced to senesce by ionizing radiation (IR), then cultured in either 10% or 0.2% serum. We also extracted lipids from mitochondrial dysfunction-associated senescent (MiDAS) cells (0.2% serum) (Wiley et al., 2016). Thus, we controlled for differences in growth state (QUI versus PRO versus SEN[IR] and MiDAS) and culture media (0.2% versus 10% serum). We measured the relative abundance of the extracted lipids by mass spectrometry.

The lipid profiles (Table S1) showed that certain subsets of lipids significantly increased or decreased upon senescence. Most notable were striking elevations in the relative abundance of oxylipins: a class of potent signaling lipids derived from 20- and 22-carbon fatty acids such as arachidonic (AA) and adrenic acid (AdA) (Figure 1A). We also observed changes in intracellular ceramides and other lipids (Table S1).

The most highly elevated senescence-associated prostaglandin was 1a,1b-dihomo-15-deoxy-Δ12,14-prostaglandin J2 (dihomo-15d-PGJ2). However, 1a,1b-dihomo- PGD2, 1a,1b-dihomo-PGE2, and other variants of prostaglandins PGD2, PGE2, and PGF2α also increased (Figure 1A). Additionally, senescent cells contained higher levels of specific leukotrienes, notably leukotriene B4 (LTB4) and the related lipoxygenase product 5-hydroxyeicosatetraenoic acid (5-HETE) (Figure 1A). Consistent with these findings, the 20-carbon oxylipin precursors AA, eicosapentaenoic acid (EPA), and dihomogamma-linoleic acid (DGLA) were elevated in senescent cells (Figure 1B).

The 22-carbon lipid AdA, a product of AA elongation (Jump, 2009; Ohno et al., 2010) and precursor of dihomo prostaglandins (Sprecher et al., 1982), also increased in senescent cells (Figure 1B). Further, senescent cells contained higher levels of the 22-carbon PUFAs docosahexaenoic acid (DHA) and docosapentaenoic acid (DPA) and the 22-carbon MUFA erucic acid, but not the 22-carbon saturated fatty acid behenic acid. Additionally, incubating senescent cells with deuterated AA resulted in an increase in deuterated AdA, confirming elongation of AA to AdA by senescent cells (Figure S1A). Thus, senescent cells show a selective and marked increase in oxylipins and elongated PUFAs and MUFAs.

To understand the mechanism by which senescent cells accumulate these lipids, we used qPCR to measure mRNA levels of several genes that function in oxylipin biosynthesis. We compared cells induced to SEN(IR), mitochondrial dysfunction (MiDAS), and RAS oncogene activation (SEN[RAS]) (Figure 1C). Among the mRNAs that increased significantly were those encoding prostaglandin synthases *PTGS2* (COX-2), *PTGDS*, *PTGES*, and *TBXAS*, but not *PTGIS*, which showed lower expression. The mRNAs encoding leukotriene biosynthetic genes, including *ALOX5* (5-LO), *ALOX15*, *ALOX5AP*, *LTC4S*, and to a lesser extent *LTA4H*, were similarly elevated. We observed similar qPCR results for oxylipin biosynthesis genes using human umbilical cord endothelial cells induced to SEN(IR) HUVECs (Figure S1B) and replicative senescent (SEN[Rep]) IMR-90 fibroblasts (Figure S1C).

To determine whether oxylipin synthesis is elevated in senescent cells *in vivo*, we used a mouse model in which $p16^{Ink4a}$-positive senescent cells can be eliminated by administration of ganciclovir (GCV) (p16-3MR mice) (Demaria et al., 2014). We treated p16-3MR mice with doxorubicin (DOXO)—an inducer of widespread senescence in mice (Demaria et al., 2017)—and measured mRNA levels of several oxylipin synthases in livers (Figure 1D). Much like cultured human cells, oxylipin synthase mRNAs increased significantly upon inducing senescence *in vivo* in mice. Further, eliminating senescent cells with GCV lowered both oxylipin synthase (Figure 1D) and $p16^{Ink4a}$ (Figure S1D) expression, confirming that the elevation was senescence-associated. Kidneys from aged mice also showed elevated levels of oxylipin synthase mRNAs (Figure S1E).

Since many oxylipins are secreted, we collected conditioned media from IMR-90 fibroblasts that were either quiescent or induced to senesce by MiDAS, ionizing radiation (SEN[IR]), or RAS oncogene activation (SEN[Ras]). Using ELISAs, we measured the levels of PGD2, which is a secreted prostaglandin that is also a precursor of 15d-PGJ2 (Figure 1E). All senescent cells showed elevated PGD2 secretion, although the ELISA does not distinguish dihomo-PGD2 from PGD2. The same was true for an epithelial-derived human cancer cell line (HEPG2; Figure 1F) and primary human umbilical vein endothelial cells (HUVECs; Figure 1G) induced to senesce by IR. Notably, hydrocortisone, a glucocorticoid that prevents AA release from intracellular membranes by activating annexin A1 (Perretti and D'Acquisto, 2009), prevented the senescence-associated release of PGD2 (Figure S1F), suggesting that the primary source of AA for prostaglandin synthesis is likely intracellular membranes. Since glucocorticoids can extend the replicative lifespan of cultured cells (Rosner and Cristofalo, 1979) and attenuate the SASP (Laberge et al., 2012), one or more AA-derived oxylipins might prevent senescence and promote the SASP.

Prostaglandins are inactivated primarily by coordinated import by a prostaglandin transporter (gene name: SLCO2A1) coupled to NAD^+-dependent oxidation of the 15(S)-hydroxyl group to an inactive 15-keto-prostaglandin metabolite by 15-hydroxyprostaglandin dehydrogenase (PGDH) (Nomura et al., 2004). Consistent with increased intracellular levels of prostaglandins (Figure 1A), *SLCO2A1* mRNA levels increased >100-fold in human fibroblasts induced to senesce by IR and mitochondrial dysfunction (Figure 1H) and >50-fold in RAS-induced senescent cells (Figure 1I). Smaller increases occurred during replicative senescence (Figure S1) and in IR-induced senescent HUVECs (Figure 1J). However, there was no commensurate increase in *PGDH* mRNA during any form of senescence (Figures 1H–1J and S1). Indeed, *PDGH* mRNA levels decreased in replicative senescent fibroblasts and IR-induced senescent HUVECs (Figures 1J and S1G). Thus, senescence entails activation of several oxylipin-synthesis pathways, especially those that generate PGD2-related lipids (Figure S1H). This activation is likely coupled to increased import without inactivation by PGDH resulting in intracellular accumulation of 15-deoxy-prostaglandins.

Dihomo-15d-pgj2 is a biomarker of senolysis in culture and *in vivo*

Since dihomo-15d-PGJ2 accumulated inside senescent cells (Figure 1A) and was not substantially secreted (Figures 2A–2D), we hypothesized that senolysis—the death of senescent cells—might release dihomo-15d-PGJ2 into the media of cultured cells and plasma of mice. To test this hypothesis,

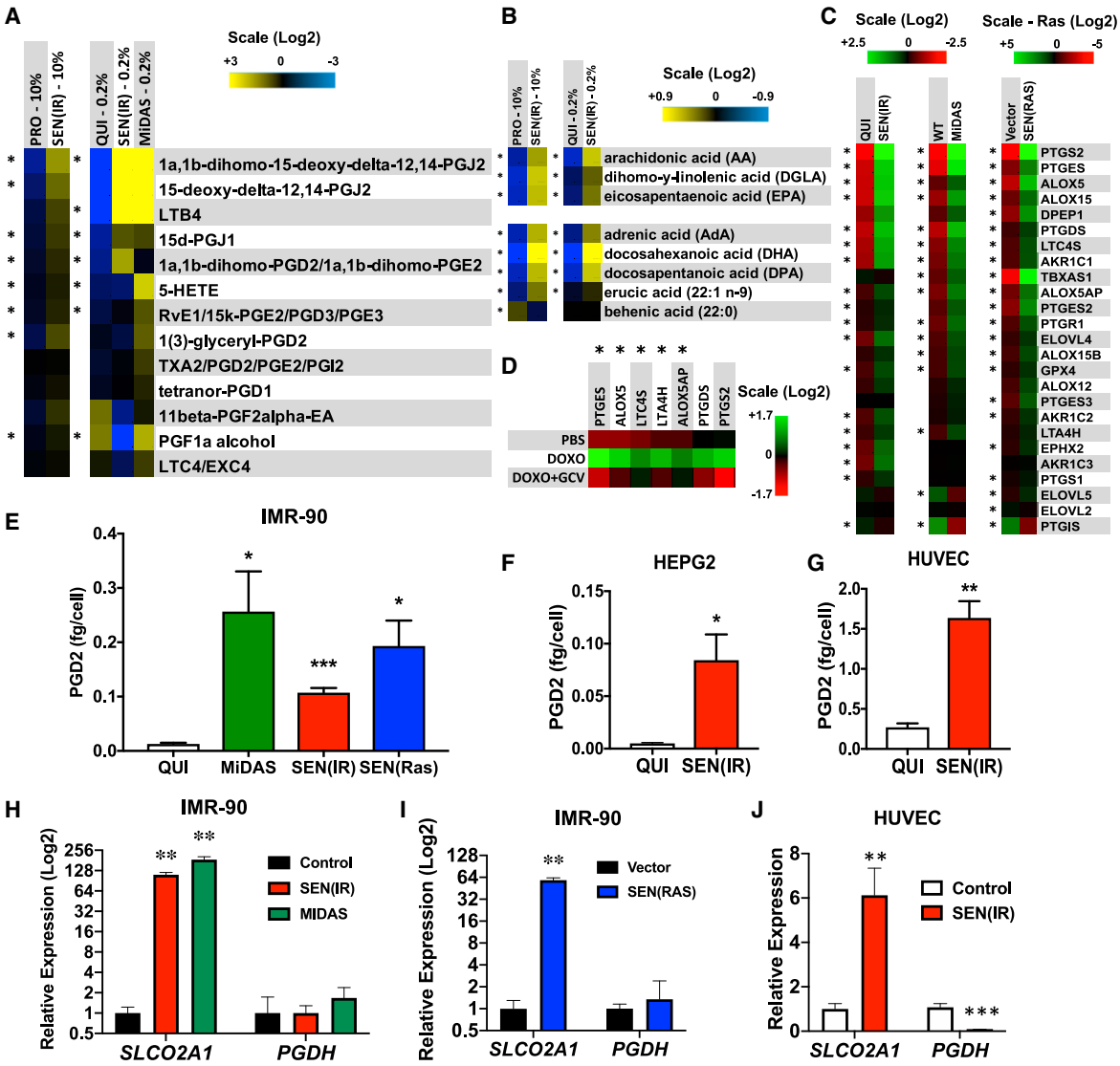

Figure 1. Senescent cells synthesize oxylipins

(A and B) IMR-90 cells were proliferative in 10% serum, made quiescent by incubation for 3 days in 0.2% serum, or made senescent by treatment with 10-Gy X-rays (IR) or ethidium bromide to induce MiDAS. Lipids were extracted from PRO (10%), QUI (0.2%), SEN(IR) (10% or 0.2% serum), or MiDAS (0.2%) cells, and analyzed by liquid chromatography-tandem mass spectrometry (LC-MS/MS). Putative oxylipins (A) and lipid precursors (B) were detected in the control and senescent cells. Heat maps indicate the averages of at least 3 experiments (*$p < 0.05$, one-way ANOVA).

(C) RNA was isolated from QUI, SEN(IR), MiDAS, and vector or RAS-V12 expressing SEN(RAS) cells, reverse transcribed, and mRNAs encoding oxylipin synthesis genes were measured by qPCR. Heat maps indicate the averages of 3 experiments (*$p < 0.05$, one-way ANOVA).

(D) p16-3MR mice were given a single dose (10 mg/kg) of DOXO or PBS by i.p. injection. After 5 days, mice were given GCV (25 mg/kg) or vehicle by i.p. injection for 5 consecutive days. Livers were harvested on day 10 and analyzed for oxylipin synthase mRNAs by qPCR. Heat maps indicate averages of at least 5 mice (*$p < 0.05$, one-way ANOVA).

(E) IMR-90 fibroblasts were induced to senesce by MiDAS, IR, or RAS-V12 overexpression. Ten days after the induction of senescence, conditioned media were collected and analyzed for PGD2 by ELISA.

(F and G) HEPG2 (F) and HUVEC (G) cells were induced to senesce by IR. Conditioned media were collected 10 days after IR and analyzed for PGD2 by ELISA. Data show means of at least 3 experiments (*$p < 0.05$, **$p < 0.01$, ***$p < 0.001$, unpaired two-tailed t test).

(H and I) RNA from (C) was analyzed for expression of SLCO2A1 or PGDH by qPCR.

(J) HUVECs were induced to senesce by IR and analyzed at Day 10 for SLCO2A1 and PGDH as in (H) and (I).

See also Figure S1 and Table S1.

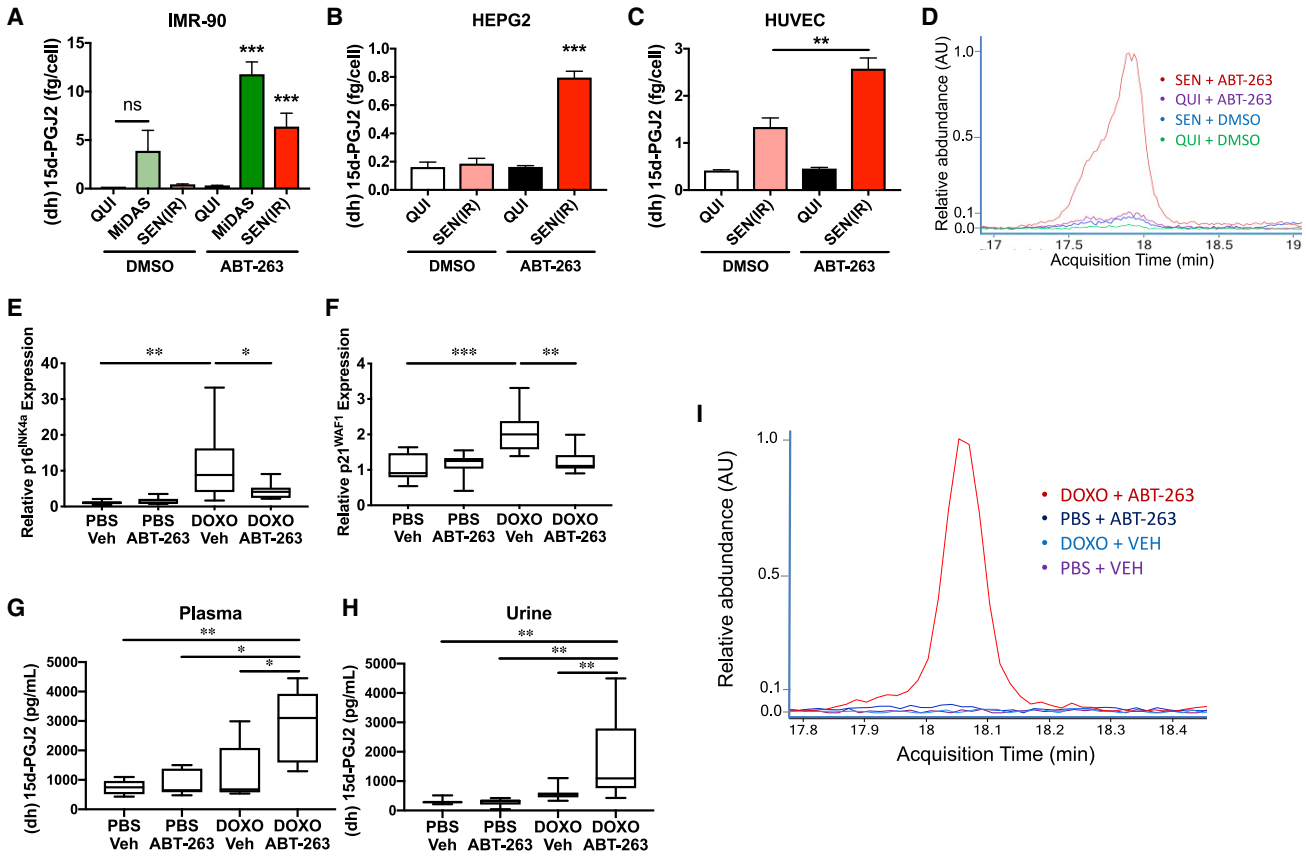

Figure 2. (Dihomo)15d-PGJ2 is a biomarker of senolysis

(A) IMR-90 fibroblasts were induced to senesce by MiDAS or IR 10 days after induction cells were treated with DMSO or 10 μM ABT-263, and (dihomo)15d-PGJ2. [(dh)-15d-PGJ2] was measured in conditioned media by ELISA. Data reflect means of at least 3 experiments.

(B and C) HEPG2 (B) or HUVEC (C) cells were induced to senesce by IR, and conditioned media from DMSO or ABT-263 treated cells were generated as in (A). (dh) 15d-PGJ2 was measured by ELISA.

(D) Representative overlay of dihomo-15d-PGJ2 peaks from extracted ion chromatograms of lipids from media treated as in (A).

(E–I) C57BL/6 mice were injected i.p. with DOXO (10 mg/kg) or PBS. Six weeks later, ABT-263 (50 mg/kg) or vehicle was administered by gavage. Data are presented as box plots for at least 6 mice per condition.

(E and F) Epididymal fat pads were harvested 3 h after ABT-263 administration and analyzed for $p16^{INK4a}$ (E) or $p21^{WAF1}$ (F) mRNA levels by qPCR.

(G) Three hours after gavage, blood was collected by cardiac puncture and (dh)15d-PGJ2 was measured by ELISA.

(H) Twelve hours after gavage, urine was collected and (dh)15d-PGJ2 was measured by ELISA.

(I) Representative overlay of dihomo-15d-PGJ2 peaks from extracted ion chromatograms of lipids extracted from plasma of the animals from (G).

*p < 0.05, **p < 0.01, ***p < 0.001, one-way ANOVA. See also Figure S2.

we cultured QUI, MiDAS, and SEN(IR) IMR-90 fibroblasts in the presence of DMSO or the senolytic drug ABT-263 (10 μM) (Chang et al., 2016). After 24 h, we collected conditioned media. At 10 μM, ABT-263 killed at least 90% of cells, regardless of senescence or quiescence. We then measured 15d-PGJ2 levels in the media by commercial ELISA, which detects both 15d-PGJ2 and dihomo-15d-PGJ2. Since the assay cannot distinguish between these lipids, we refer to the ELISA signal as "(dh)15d-PGJ2" to acknowledge that this signal may come from either lipid. Media from MiDAS cells, which have a low basal level of apoptosis, showed some (dh)15d-PGJ2, but this increased significantly when the cells were treated with ABT-263 (Figure 2A). Similarly, SEN(IR) media contained only small amounts of (dh)15d-PGJ2 but contained much more after ABT-263-mediated senolysis (Figure 2A).

To determine whether (dh)15d-PGJ2 predicted senolysis in other cell lineages, we measured its release upon ABT-263-induced senolysis in senescent HEPG2 and HUVEC cells. In each case, senolysis increased (dh)15d-PGJ2 (Figures 2B and 2C). Senescent HUVECs showed some (dh)15d-PGJ2 when vehicle treated (Figure 2C), but since some HUVECs detach from the plate and undergo anoikis during routine culture, this elevation was expected. Since the ELISA antibody was raised against 15d-PGJ2, not specifically dihomo-15d-PGJ2, we used mass spectrometry to determine whether dihomo-15d-PGJ2 was released by senescent cells. We assayed conditioned media from QUI+DMSO, SEN(IR)+DMSO, QUI+ABT-263, and SEN(IR)+ABT-263 cells. In agreement with Figure 1A and the ELISA data, we detected substantially elevated dihomo-15d-PGJ2 only in SEN(IR)+ABT-263 cells (Figure 2D). By comparison, non-senescent IMR-90s did not release dihomo-15d-PGJ2

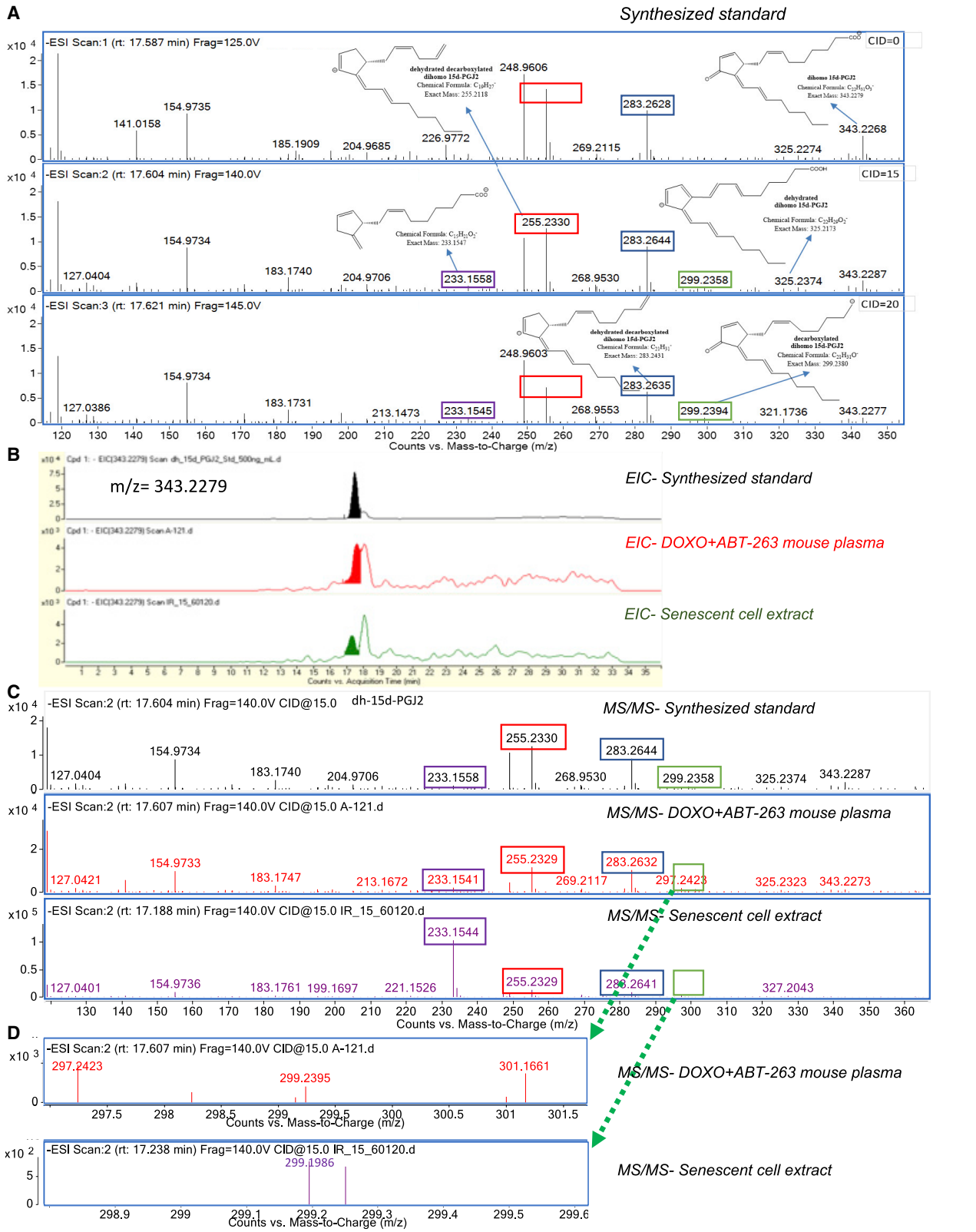

Figure 3. Validation of dihomo-15d-PGJ2 as a biomarker of senolysis

(A) A synthesized dihomo-15dPGJ2 standard was analyzed at 3 different voltages for fragmentation patterns. Key identification peaks included 299.2 *m/z* (C21H31O$^-$: green box), 283.2 *m/z* (C21H31$^-$: blue box), 255.2 *m/z* (C19:H27$^-$: red box), and 233.2 *m/z* (C15H21O2$^-$: purple box).

(legend continued on next page)

when treated with non-selective apoptosis inducers (staurosporine or TRAIL) (Figure S2A), indicating that dihomo-15d-PGJ2 is a distinct feature of senolysis in culture.

To determine whether dihomo-15d-PGJ2 could be used to detect senolysis *in vivo*, we treated mice with DOXO and allowed them to accumulate senescent cells over 6 weeks, as described (Demaria et al., 2017). We then administered ABT-263 (50 mg/kg) by gavage (Chang et al., 2016). After 3 h, mRNA levels of $p16^{Ink4a}$ and $p21^{Waf1}$ declined significantly in the epididymal fat of ABT-263-treated mice (Figures 2E and 2F). Further, ELISAs showed elevated (dh)15d-PGJ2 in the plasma of DOXO + ABT-263 treated mice, but not control mice (Figure 2G). Similarly, 12 h after ABT-263-induced senolysis, urine (dh)15d-PGJ2 was elevated relative to controls (Figure 2H). Ion chromatograms from mouse plasma from DOXO + ABT-263 mice revealed the 343 *m/z* peak indicative of dihomo-15d-PGJ2 (Figures 2I and S2B), which was absent from plasma from PBS + vehicle, PBS + ABT-263, and DOXO + vehicle mice (Figures 2I and S2C). We did not detect a (non-dihomo)15d-PGJ2 peak in plasma from any treatment group examined (Figure S2D). We conclude that senolysis is accompanied by the release of dihomo-15d-PGJ2 from senescent cells *in vivo*.

Dihomo-15d-PGJ2 was highly elevated and abundant (~1–5 μM) in senescent cells but is considerably unstudied (detected in one published list of analytes) (Lee et al., 2016). To confirm its identity, we obtained a synthetic dihomo-15d-PGJ2 standard (Jubilant Chemsys; 94% purity) (Figures S3A and S3B) and used it to confirm the identity of the senolysis biomarker. Dihomo-15d-PGJ2 differs from 15-PGJ2 by an additional C_2H_4 group, resulting in a mass shift of 28 Da (from 315.2 to 343.2 *m/z*) (Figure S2B). In addition, the MS/MS fragmentation patterns of the standard (Figure 3A) revealed peaks at 299.2 *m/z* (loss of CO_2), 283.3 *m/z* (loss of $CO_2 + H_2O$), 255.2 (loss of $CO_2 + H_2O + C_2H_4$), and 233.2 (loss of $H_2O + C_7H_8$). Retention times between the dihomo-15d-PGJ2 standard and samples from senolytic-treated culture or plasma samples closely matched (Figure 3B; filled peaks). Samples also showed a second peak at a later time that was not specific to senolysis (Figure 3B; unfilled peaks). Analysis of the senolysis-specific peaks by MS/MS fragmentation revealed characteristic peaks at 283.3, 255.2, and 233.2 *m/z* (Figure 3C), as well as the 299.2 *mz* peak (presented separately in Figure 3D). Together, these peaks confirmed that dihomo-15d-PGJ2 was the senolysis-released lipid detected in our analyses.

Prostaglandins promote senescent phenotypes

To understand the consequence of senescence-associated oxylipin biosynthesis, we considered that cyclooxygenase 2 (Ptgs2) overexpression causes premature aging phenotypes in mice (Kim et al., 2016), and oxylipin synthesis inhibitors extend male mouse lifespan (Strong et al., 2008). To determine whether prostaglandin synthesis promotes senescent phenotypes, we treated irradiated cells (SEN[IR])with either of two prostaglandin synthase 2 (PTGS2/COX-2) inhibitors: CAY-10404 (CAY) or NS-398 (NS), which delays replicative senescence (Han et al., 2004). Both inhibitors suppressed secreted PGD2 levels, as determined by ELISA (Figure 4A). Notably, when counting cells for normalization (Figure 4A), SEN(IR) cells exposed to either inhibitor showed an increased cell number relative to control cells (Figure S4A). This finding suggests that prostaglandin biosynthesis might reinforce the senescence proliferative arrest.

To address this possibility, we irradiated IMR-90 fibroblasts with a lower IR dose (5 Gy versus 10 Gy), which causes a senescence growth arrest in 90% versus >99% of cells, and treated them with CAY or NS. CAY and to a greater degree NS significantly increased EdU incorporation (Figure 4B), decreased senescence-associated beta-galactosidase (SA-Bgal) positivity (Figure 4C), and decreased both *CDKN1A* (p21) and *CDKN2A* ($p16^{INK4a}$) mRNA levels (Figures 4D and 4E).

Most prostaglandins and leukotrienes are secreted and many can promote cell proliferation and inflammation (Castellone et al., 2005; Dennis and Norris, 2015; Ricciotti and FitzGerald, 2011). Thus, the senescence-associated oxylipins we detected might drive the inflammatory arm of the SASP. To test this idea, we inhibited prostaglandin synthesis with CAY or NS in SEN(IR) cells and measured secreted levels of the pro-inflammatory SASP factor interleukin 6 (IL-6) (Figure 4F). Both compounds reduced secreted IL-6 levels (Figure 4F).

To assess the effects on other SASP factors, we extracted mRNA from each treatment group and measured gene expression by qPCR. COX-2 inhibition by either compound decreased mRNA levels of all the inflammatory cytokines assayed, as well as *MMP3*, but did not affect *VEGF*, part of a pro-angiogenic subset of SASP factors (Figure 4G). COX-2 inhibition similarly affected cell number, IL-6 secretion, EdU incorporation, and colony formation in oncogenic RAS-induced senescent cells (Catalano et al., 2005; Serrano et al., 1997) (Figures S4B–S4F). Thus, prostaglandin synthesis promotes phenotypes associated with senescence, including cell-cycle arrest and the expression and secretion of certain SASP factors.

Dihomo-15d-PGJ2 markedly increased in senescent cells, suggesting this lipid and/or similar cyclopentenone prostaglandins might drive senescence phenotypes. To test this idea, we treated non-senescent cells with 15d-PGJ2 or dihomo-15d-PGJ2 and measured markers of senescence. Both lipids reduced EdU incorporation (Figure 4H) and *LMNB1* mRNA (Figure 4M) and increased SA-Bgal activity (Figures 4I and 4J) and *CDKN1A/p21* mRNA levels (Figure 4K). Only dihomo-15d-PGJ2 increased *CDKN2A/p16* mRNA (Figure 4L). Further, although both lipids induced several SASP factor mRNAs, dihomo-15d-PGJ2 induced higher levels of these mRNAs than 15d-PGJ2 (Figure 4N). Both lipids also induced PTGS2/COX-2,

(B) Extracted ion chromatograms from a dihomo-15d-PGJ2 standard (top), plasma from a DOXO+ABT-263 mouse (middle), and senescent cell extracts (bottom). Filled peaks appeared only in senolysis (middle) or senescence (bottom).
(C) Fragmentation patterns of filled peaks from (B) indicating a dihomo-15d-PGJ2 standard (top), plasma from a DOXO+ABT-263 mouse (middle), or senescent cell extracts (bottom).
(D) Zoomed chromatograms for the 299.2 *m/z* peaks (zoomed area indicated by green boxes in C) in DOXO + ABT-263 mouse plasma (upper) or senescent cell extracts (lower). Note that the relative abundance of a non-specific peak (unfiled in Figure 3B) required earlier fragmentation in SEN(IR) extracts.
See also Figure S3.

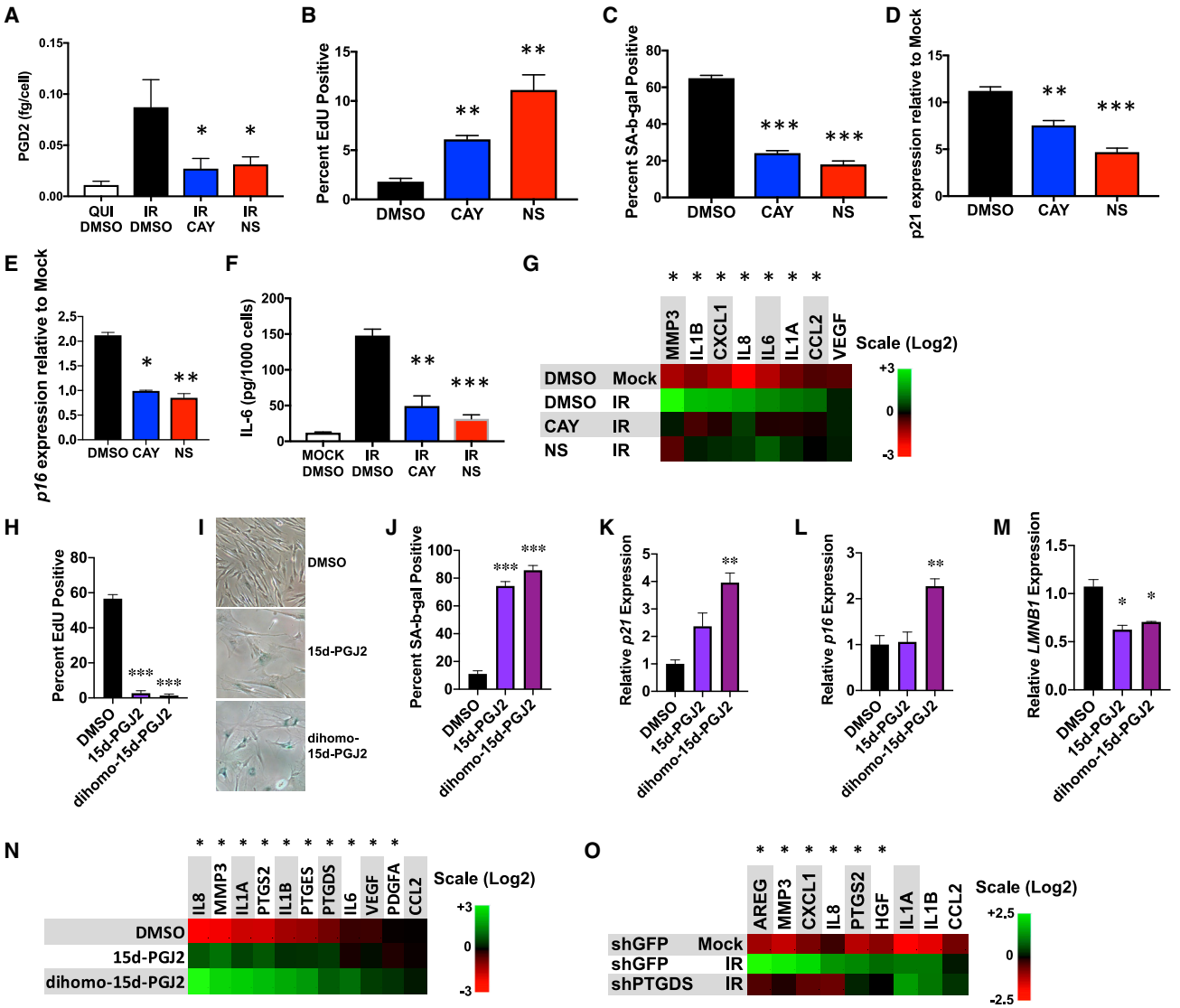

Figure 4. Prostaglandins promote cellular senescence phenotypes

(A–F) IMR-90 fibroblasts were induced to senesce by IR and treated with DMSO or COX-2 inhibitors CAY-10404 (CAY) or NS-398 (NS) for 10 days.

(A) Conditioned media were harvested and secreted PGD2 was measured by ELISA.

(B) Twenty-four hour EdU incorporation for irradiated cells in each treatment group.

(C) SA-Bgal positivity for irradiated cells in each treatment group.

(D) p21 mRNA levels in each treatment group.

(E) p16 mRNA levels from each treatment group.

(F) Conditioned media from (A) were analyzed for IL-6 secretion by ELISA.

(G) mRNA levels of genes encoding SASP factors from all treatment groups were measured by qPCR.

(H–N) Proliferating cells were cultured for 10 days in the presence of DMSO or 5 μM 15d-PGJ2 or dihomo-15d-PGJ2.

(H) Twenty-four hour EdU labeling indices for each treatment.

(I) Example of SA-Bgal-positive cells after each treatment. Panels are cropped zooms to larger images and red saturation has been lowered for all images to allow visualization of the blue X-gal staining.

(J) SA-Bgal positivity for each treatment.

(K) p21 mRNA levels in extracts from prostaglandin- and DMSO-treated cells.

(L) $p16^{INK4a}$ mRNA levels in extracts from prostaglandin- and DMSO-treated cells.

(M) *LMNB1* mRNA levels in extracts from prostaglandin- and DMSO-treated cells.

(N) SASP factor PTGS2, PTGDS, and PTGES mRNA levels were measured by qPCR. Normalized to actin.

(O) Cells were transduced with lentiviruses expressing shRNA targeting either GFP (shGFP; control) or PTGDS (shPTGDS), irradiated as in (A), and mRNA extracted 10 days after irradiation. SASP gene expression was measured by qPCR.

Bar graphs indicate averages of at least 3 experiments (*$p < 0.05$, **$p < 0.01$, ***$p < 0.001$, unpaired two-tailed t test). Heatmaps indicate averages of 3 experiments (*$p < 0.05$, two-way ANOVA). See also Figure S4.

PTGES, and PTGDS mRNAs, suggesting a positive feedback loop maintains prostaglandin synthesis and senescence phenotypes. PGD2 and PGJ2 had similar effects on senescence phenotypes (Figures S4G–S4L), as did PGE2 to a lesser degree, as reported (Martien et al., 2013). In agreement with positive feedback by prostaglandins, PTGS2/COX-2 expression declined upon inhibition of COX-2 with NS or CAY (Figure S4M). Phenotypes induced by PGE2 were unlikely due to senescence, as cells treated with PGE2, but not PGD2 or PGJ2, became smaller and resumed proliferation once PGE2 was removed (Figures S4N and S4O). Thus, PGD2 and related metabolites can promote senescence.

To further test this idea, we depleted prostaglandin D synthase (PTGDS) by lentiviral-delivered short hairpin RNA (shRNA) (shPTGDS) and measured mRNA levels of SASP factors following induction of senescence by IR. One shRNA efficiently reduced PTGDS expression (Figure S4P) and also reduced several SASP factor mRNAs compared with senescent cells transduced with a control shRNA (shGFP) (Figure 4O). Together with Figures 4H–4N, we conclude that PGD2 and related lipids promote cellular senescence phenotypes.

Extracellular PGD2 signals through two receptors, DP1 (*PTGDR*) and DP2 (*PTGDR2*) (Hata and Breyer, 2004; Ricciotti and FitzGerald, 2011); 15d-PGJ2 preferentially binds DP2 (Monneret et al., 2002; Ricciotti and FitzGerald, 2011). To determine whether either receptor drives senescence, we treated non-senescent cells with PGD2, a DP1-specific agonist (BW245C) (Town et al., 1983), a DP2-specific agonist (13,14-dihydro-15-keto-PGD2) (Hirai et al., 2001), and both agonists or vehicle (DMSO). The DP1 agonist increased cyclic AMP (cAMP) levels, while the DP2 agonist lowered cAMP levels (Figure S5A), confirming receptor activation (Hata and Breyer, 2004; Hirai et al., 2001, Hirata et al., 1994; Ricciotti and FitzGerald, 2011). PGD2 did not affect cAMP levels (Figure S5A). Both the DP1 agonist and PGD2 reduced EdU incorporation but only PGD2 elevated SA-Bgal activity (Figure S5B). PGD2 also increased mRNAs encoding p21 and $p16^{INK4a}$ (Figures S5C and S5D), whereas the DP1 agonist lowered these mRNA levels. The DP2 agonist had no effect. Although *PTGDR* mRNA levels were unchanged between senescent and non-senescent cells, *PTGDR2* mRNA was ~50-fold lower in senescent cells and, thus, unlikely to affect senescence (Figure S5D). PGD2 induced many mRNAs encoding SASP factors, but the DP1 agonist did not (Figure S5F). Finally, we treated cells with either a DP1 (BW-A868C) (Giles et al., 1989) or DP2 (OC000459) (Pettipher et al., 2012) antagonist for 10 days after inducing senescence by IR. Neither antagonist altered SASP gene expression (Figure S5G). These data indicate that PGD2 and its derivatives do not drive senescence through classic prostaglandin D2 receptor signaling, consistent with requirements for μM concentrations (these receptors typically require nM concentrations). We therefore sought to identify alternative pathways.

15d-PGJ2 is the dehydration product of PGD2 (Forman et al., 1995; Kliewer et al., 1995), and dihomo-15d-PGJ2 is the most highly elevated prostaglandin inside senescent cells (Figure 1A). Therefore, we tested the possibility that intracellular dihomo-15d-PGJ2 promotes senescence, independent of cell surface receptor signaling. 15d-PGJ2 is a ligand for PPAR-γ (Forman et al., 1995; Kliewer et al., 1995), which is linked to senescence (Gan et al., 2008). We transduced IMR-90 fibroblasts with a baculovirus containing a luciferase PPAR-γ reporter and measured its activity in quiescent and SEN(IR) cells cultured in DMSO or the prostaglandin synthase inhibitor NS-398. PPAR-γ reporter activity increased ~18-fold upon senescence, and NS-398 lowered this activity by ~50% (Figure S5H), indicating that PPAR-γ activation is partially dependent on prostaglandin synthesis in senescent cells. We then cultured cells with two PPAR-γ agonists—ciglitazone (20 μM) or troglitazone (20 mM)—for 10 days. Unlike 15d-PGJ2, neither agonist induced senescence, as determined by EdU incorporation and SA-Bgal activity (Figure S5**I**). Therefore, while prostaglandin synthesis indeed activates PPAR-γ in senescent cells, PPAR-γ does not drive senescence phenotypes.

Prostaglandins reinforce senescence via positive ras/p53 feedback

H-RAS is activated by exogenous 15d-PGJ2 at 3–5 μM (Oliva et al., 2003), roughly the dihomo-15d-PGJ2 level at which senescent cells and other cyclopentenone prostaglandins activate other RAS isoforms or similar GTPases (Anta et al., 2016; Renedo et al., 2007; Wall et al., 2015). We hypothesized that constitutive RAS activation might drive senescence in response to the elevated dihomo-15d-PGJ2. Indeed, incubation of quiescent cells with 15d-PGJ2 resulted in RAS activation, as well as phosphorylation of the downstream effector kinases ERK1/2 (Figure 5A; left lanes) (Oliva et al., 2003). Consistent with elevated 15d-PGJ2 levels, SEN(IR) cells showed increased RAS activation (RAS: guanosine triphosphate [GTP]) and phospho-ERK1/2, which was attenuated by CAY or NS (Figure 5A). Similarly, shRNA-mediated knockdown of PTGDS (shPTGDS) selectively prevented RAS activation (Figure 5A). RAS activation is also associated with loss of intracellular dNTPs due to suppression of *RRM2* expression (Aird et al., 2013). A similar loss of *RRM2* occurred in IR-induced senescence, which was prevented by CAY or NS (Figure 5B). Importantly, administration of deuterated 15d-PGJ2 resulted in roughly equimolar accumulation of deuterated 15d-PGJ2 inside senescent cells (Figure S5**J**), demonstrating that exogenously administered prostaglandins can accumulate intracellularly at levels that approximate those found in senescent cells.

RAS-induced senescence is driven by a mitogen-activated kinase (MAPK) cascade, resulting in p53 phosphorylation on serine 37 (p53-S37) by a p38-regulated activated kinase (PRAK/MAPKAPK5) (Sun et al., 2007). Indeed, PRAK was phosphorylated on threonine 182 (PRAK-R182), p53 was phosphorylated on serine 37 and p21 protein levels increased in cells induced to senesce by 15d-PGJ2 (Figures 5C and 5D). These data suggest that 15d-PGJ2 reinforces senescence through a RAS-driven pathway.

H-RAS knockdown was toxic, so we used a RAF inhibitor (AZ 628) (Montagut et al., 2008) to block downstream RAS signaling. AZ 628 (20, 5, or 1 μM) strongly inhibited ERK phosphorylation in response to serum stimulation without affecting basal levels of p53 or p21 (Figure S5K). Further, 1 μM AZ 628 did not alter SA-b-gal activity (Figures S5L and S5M) or EdU labeling (Figure S5N). We, therefore, used 1 μM for further studies. In response to 15d-PGJ2, AZ 628 blocked ERK1/2 and p53 phosphorylation thus preventing the rise in p53 and p21 proteins

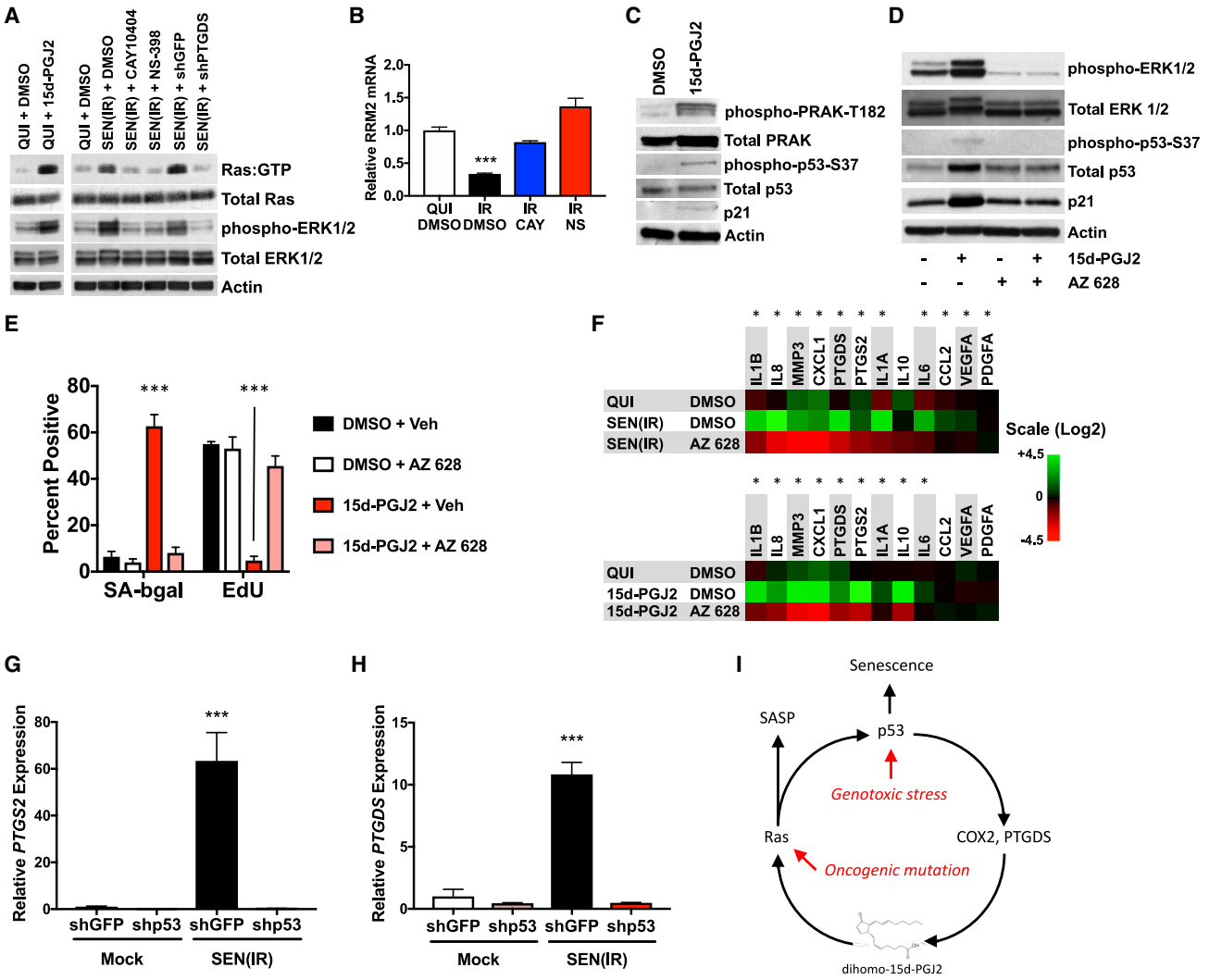

Figure 5. 15d-PGJ2 promotes senescent phenotypes by activating RAS

(A) Extracts from IMR-90 fibroblasts were analyzed for activated RAS (Ras:GTP), total Ras, phospho-ERK1/2, total ERK1/2, and actin by immunoblot. Left: quiescent cells were treated with DMSO or 5 μM 15d-PGJ2 for 15 min before harvest. Right: cells were induced to senesce by 10 Gy IR and treated with DMSO, CAY-10404, NS-398, or lentiviral shRNAs to GFP (shGFP) or PTGDS (shPTGDS). Cells were cultured for 10 days prior to harvest, and in 0.2% fetal bovine serum FBS for the last 48 h.

(B) Cells were induced to senesce by 5 Gy IR and cultured in the presence of vehicle (DMSO), CAY, or NS for 10 days. RNA was extracted, reverse-transcribed, and analyzed for RRM2 mRNA relative to actin mRNA by qPCR.

(C) Immunoblot of cells treated with DMSO or 10 μM 15d-PGJ2 for 10 days. Blots were probed for phospho-PRAK-T182, total PRAK, phospho-p53-S37, and total p53, p21 and actin.

(D) Cells were treated with vehicle or 15d-PGJ2, and DMSO or AZ 628 for 10 days. Protein was extracted and analyzed by immunoblot for phospho-ERK1/2, total ERK1/2, phospho-p53-S37, and total p53, p21, and actin.

(E) Cells treated as in (D) were analyzed for SA-Bgal or 24 h EdU incorporation.

(F) Cells were induced to senesce by 10 Gy IR or continuous culture with 10 μM 15d-PGJ2 for 10 days. DMSO or AZ 628 was concurrently added from day 0 and present until day 10. Quiescent cells cultured in DMSO served as a control. RNA was then extracted and analyzed by qPCR for mRNAs encoding SASP factors, PTGS2 and PTGDS.

(G and H) Cells were transduced with lentiviral shRNAs to either GFP (shGFP) or p53 (shp53), mock irradiated or given 10 Gy IR, and cultured for 10 days (shGFP) or 3 days (shp53) before RNA extraction and analysis for (G) PTGS2 or (H) PTGDS mRNAs.

(I) Model for a feedback loop involving 15d-PGJ2, RAS, and p53 that reinforces senescent phenotypes. Chemiluminescent western images were captured with either film or by Bio-Rad Gel-Doc. Image formats may therefore be inconsistent between lanes within panels.

Bar graphs indicate averages of at least 3 experiments (***$p < 0.001$, unpaired two-tailed t test). Heatmaps indicate averages of 3 experiments (*$p < 0.05$, two-way ANOVA). See also Figure S5.

(Figure 5D). AZ 628 also prevented the rise in SA-Bgal and decline in EdU labeling in response to 15d-PGJ2 (Figure 5E). Finally, continuous culture of either SEN(IR) or 15d-PGJ2-treated cells with AZ 628 prevented much of the rise in pro-inflammatory SASP factor mRNAs, lowered levels of both *PTGS2* and *PTGDS* mRNAs, and thus antagonized the positive feedback initiated by 15d-PGJ2 (Figure 5F). AZ 628 also prevented the rise in mRNAs encoding p21 and $p16^{INK4a}$ and reduction in *LMNB1* mRNA in response to 10 Gy IR (Figures S5**O–S5Q**). Thus, activation of the RAS pathway is a key step in the development of senescent phenotypes, even in the absence of activating mutations.

Since 15d-PGJ2 activated p53 (S37 phosphorylation) and COX-2/PTGS2 inhibitors lowered *PTGS2* mRNA levels in senescent cells (Figure S4**M**), we tested the possibility that p53 is required for the increased expression of prostaglandin synthase enzymes. Indeed, p53 depletion by a lentiviral shRNA (shp53) completely abolished *PTGS2* and *PTGDS* expression in response to IR (Figures 5G and 5H). *CDKN1A/p21* expression was similarly attenuated, as expected (Figure S5**R**). By comparison, depletion of the NF-κB subunit RELA using a lentiviral shRNA (shRELA) had no effect on prostaglandin synthase expression (Figures S5S **and S5T**), despite lowering *IL6* expression (Figure S5**U**), as described (Freund et al., 2011). Thus, activation of p53 or RAS results in a positive feedback loop that promotes senescence and segments of the SASP by activating prostaglandin synthesis (Figure 5I). Given that prostaglandin synthesis is required for senescence, the data indicate that prostaglandin-mediated RAS activation is a common and necessary feature of at least some forms of cellular senescence.

DISCUSSION

Our results indicate that oxylipins are a lipid-based component of the SASP. Secretion of these lipids likely has significant physiological effects, apart from the cell-autonomous role of dihomo-15d-PGJ2. For example, chorioamnion-derived PGE2 and PGF2α are key signals for parturition (Gibb, 1998) and senescent cells appear in the chorioamniotic membranes of women in labor (Behnia et al., 2015; Menon et al., 2016), suggesting that senescent cells may be a source of parturition-inducing prostaglandins.

Importantly, we observe the intracellular accumulation of cyclopentenone prostaglandins, such as dihomo-15d-PGJ2. This accumulation was linked to the increased expression of the prostaglandin transporter but not prostaglandin dehydrogenase, which might explain the accumulation of 15-deoxy prostaglandins. Increased import without a commensurate change in PGDH might promote the cytoplasmic accumulation of dehydrated 15-deoxy prostaglandins, rather than 15-keto prostaglandins.

Given that elevated intracellular dihomo-15d-PGJ2 and its biosynthetic enzymes occur in several cell types and tissues in response to multiple senescence inducers, we propose that the synthesis of dihomo-15d-PGJ2 and RAS activation are common features of senescent cells. While oncogenic RAS mutations are known to drive cells into senescence (Serrano et al., 1997), our studies identify a role for wild-type RAS in senescence. We show that the RAS-RAF signaling pathway is important for many aspects of senescence, including components of the SASP, increased levels of p21 and $p16^{INK4a}$, and decline in lamin B1 levels.

We previously showed that p53 restrains segments of the SASP by antagonizing NF-kB signaling (Freund et al., 2011; Wiley et al., 2018). Here, we show that p53 is required for prostaglandin biosynthesis, and inhibition of prostaglandin synthesis antagonizes the SASP. These findings explain why p53 does not completely prevent the SASP. Thus, inhibition of prostaglandin synthesis did not return inflammatory cytokine levels to those of non-senescent cells, unlike *RELA* depletion, suggesting that prostaglandins contribute to, but are not exclusively necessary for, the secretion of pro-inflammatory factors. The role of p53-dependent prostaglandin synthesis in the development of the SASP is likely overshadowed by the loss of NF-kB antagonism when p53 is depleted, resulting in increased inflammatory cytokine secretion in the absence of p53, even when prostaglandin synthesis is lost.

Senescence and the SASP are dynamic phenotypes that change over time (De Cecco et al., 2019; Hernandez-Segura et al., 2017). The lipids described here likely undergo dynamic regulation as well. Indeed, we recently showed that the expression of specific lipid synthases is temporally regulated in the context of pulmonary fibrosis, suggesting a transition from acute to more chronic stress phenotypes (Wiley et al., 2019a).

Finally, our finding that released dihomo-15d-PGJ2 can be used as a biomarker for senolysis has several potential applications. Senolytic drugs are increasingly being used in aging and related research and—importantly—have entered early clinical trials (Hickson et al., 2019; Justice et al., 2019). Determining that senolysis is taking place is essential for evaluating these compounds as therapeutic agents. Detection of dihomo-15d-PGJ2 in biological fluids may allow rapid evaluation of the efficacy of these compounds.

Limitations of study

Outside of dihomo-15d-PGJ2, most of the factors in Figures 1A and 1B are assigned by *m/z* and therefore are only likely assignees. We list these factors in the figure legend as "putative" as a result. This study only features analyses from mice and human cells, and for 3 cell types as representatives of endothelial, epithelial, and mesenchymal lineages. Results may not reflect all lineages or inducers of senescence.

STAR★METHODS

Detailed methods are provided in the online version of this paper and include the following:

- KEY RESOURCES TABLE
- RESOURCE AVAILABILITY
  - Lead contact
  - Material availability
- DATA AND CODE AVAILABILITY
- EXPERIMENTAL MODEL AND SUBJECT DETAILS
  - Cell lines and strains
  - Animals
- METHOD DETAILS
  - Gene expression
  - Induction of senescence

- Generation of conditioned media
- Induction of apoptosis or senolysis
- Senescence-associated beta-galactosidase
- Colony forming assay
- RAS activation assay
- Immunoblots
- IL-6 ELISA
- PGD2-MOX ELISA
- 15d-PGJ2 ELISA
- Reporter assays
- Chemicals and standards
- Liquid-liquid extraction (LLE) of lipids
- Solid phase extraction (SPE) of lipids
- High-pressure liquid chromatography quadrupole-time-of-flight mass spectrometry (HPLC-QTOF-MS)
- High-pressure liquid chromatography quadropole ion trap mass spectrometry (HPLC-QTRAP-MS)
- Reverse-phase LC-MS method for detection of 15d-PGJ2
- Quantitation of intracellular dihomo-15d-PGJ2 concentration

● QUANTIFICATION AND STATISTICAL ANALYSIS

- Data representation and statistical analysis

SUPPLEMENTAL INFORMATION

Supplemental information can be found online at https://doi.org/10.1016/j.cmet.2021.03.008.

ACKNOWLEDGMENTS

The authors thank Peiqing Sun for the gift of the phospho-PRAK antibody and Pierre-Yves Desprez for the critical reading of this manuscript. This work was supported by grants from the National Institutes of Health (AG051729, AG057353, AG0172442, U2C-DK119886, and T32-AG000266) and the Science and Engineering Research Board of India (DST- SERB SPR/2019/001265).

AUTHOR CONTRIBUTIONS

C.D.W. and A. Ramanathan conceived, designed, and interpreted the lipid profiling experiments. S.S.D. and R.S. designed and conducted all mass spectrometry experiments with guidance from A. Ramanathan; A. Ramanathan, R.S., and A. Rosko conducted post-experiment informatics and interpretation. S.S.D., K.P.M., S.W., and S.M.D. extracted lipids and conducted analyses. C.D.W., J.A.L.-D., F.A., D.E.K., and M.D. conducted mouse experiments. E.A., F.N., and C.K. conducted additional assays. All other experiments were designed and conducted by C.D.W. with guidance from A. Ramanathan and J.C.; C.W., A. Ramanathan, R.S., and J.C. wrote the paper and addressed reviewer comments.

DECLARATION OF INTERESTS

J.C. is a founder of Unity Biotechnology, which develops senolytic therapies. C.W., A.R., and J.C. are inventors on a patent for the detection of oxylipins as biomarkers of senolysis.

Received: January 16, 2020
Revised: September 21, 2020
Accepted: March 11, 2021
Published: April 2, 2021

REFERENCES

Acosta, J.C., O'Loghlen, A., Banito, A., Guijarro, M.V., Augert, A., Raguz, S., Fumagalli, M., Da Costa, M., Brown, C., Popov, N., et al. (2008). Chemokine signaling via the CXCR2 receptor reinforces senescence. Cell *133*, 1006–1018.

Aird, K.M., Zhang, G., Li, H., Tu, Z., Bitler, B.G., Garipov, A., Wu, H., Wei, Z., Wagner, S.N., Herlyn, M., and Zhang, R. (2013). Suppression of nucleotide metabolism underlies the establishment and maintenance of oncogene-induced senescence. Cell Rep *3*, 1252–1265.

Anta, B., Pérez-Rodríguez, A., Castro, J., García-Domínguez, C.A., Ibiza, S., Martínez, N., Durá, L.M., Hernández, S., Gragera, T., Peña-Jiménez, D., et al. (2016). PGA1-induced apoptosis involves specific activation of H-Ras and N-Ras in cellular endomembranes. Cell Death Dis *7*, e2311.

Baker, D.J., Childs, B.G., Durik, M., Wijers, M.E., Sieben, C.J., Zhong, J., Saltness, R.A., Jeganathan, K.B., Verzosa, G.C., Pezeshki, A., et al. (2016). Naturally occurring p16(Ink4a)-positive cells shorten healthy lifespan. Nature *530*, 184–189.

Behnia, F., Taylor, B.D., Woodson, M., Kacerovsky, M., Hawkins, H., Fortunato, S.J., Saade, G.R., and Menon, R. (2015). Chorioamniotic membrane senescence: a signal for parturition? Am. J. Obstet. Gynecol. *213*, 359.e1–359.e6.

Bligh, E.G., and Dyer, W.J. (1959). A rapid method of total lipid extraction and purification. Can. J. Biochem. Physiol. *37*, 911–917.

Buratta, S., Urbanelli, L., Sagini, K., Giovagnoli, S., Caponi, S., Fioretto, D., Mitro, N., Caruso, D., and Emiliani, C. (2017). Extracellular vesicles released by fibroblasts undergoing H-Ras induced senescence show changes in lipid profile. PLoS One *12*, e0188840.

Cadenas, C., Vosbeck, S., Hein, E.M., Hellwig, B., Langer, A., Hayen, H., Franckenstein, D., Büttner, B., Hammad, S., Marchan, R., et al. (2012). Glycerophospholipid profile in oncogene-induced senescence. Biochim. Biophys. Acta *1821*, 1256–1268.

Campisi, J. (2013). Aging, cellular senescence, and cancer. Annu. Rev. Physiol. *75*, 685–705.

Castellone, M.D., Teramoto, H., Williams, B.O., Druey, K.M., and Gutkind, J.S. (2005). Prostaglandin E2 promotes colon cancer cell growth through a Gs-axin-beta-catenin signaling axis. Science *310*, 1504–1510.

Catalano, A., Rodilossi, S., Caprari, P., Coppola, V., and Procopio, A. (2005). 5-Lipoxygenase regulates senescence-like growth arrest by promoting ROS-dependent p53 activation. EMBO J *24*, 170–179.

Chang, J., Wang, Y., Shao, L., Laberge, R.M., Demaria, M., Campisi, J., Janakiraman, K., Sharpless, N.E., Ding, S., Feng, W., et al. (2016). Clearance of senescent cells by ABT263 rejuvenates aged hematopoietic stem cells in mice. Nat. Med. *22*, 78–83.

Coppé, J.P., Patil, C.K., Rodier, F., Sun, Y., Muñoz, D.P., Goldstein, J., Nelson, P.S., Desprez, P.Y., and Campisi, J. (2008). Senescence-associated secretory phenotypes reveal cell-nonautonomous functions of oncogenic RAS and the p53 tumor suppressor. PLoS Biol *6*, 2853–2868.

Cormenier, J., Martin, N., Deslé, J., Salazar-Cardozo, C., Pourtier, A., Abbadie, C., and Pluquet, O. (2018). The ATF6alpha arm of the unfolded protein response mediates replicative senescence in human fibroblasts through a COX2/prostaglandin E2 intracrine pathway. Mech. Ageing Dev. *170*, 82–91.

Dagouassat, M., Gagliolo, J.M., Chrusciel, S., Bourin, M.C., Duprez, C., Caramelle, P., Boyer, L., Hue, S., Stern, J.B., Validire, P., et al. (2013). The cyclooxygenase-2-prostaglandin E2 pathway maintains senescence of chronic obstructive pulmonary disease fibroblasts. Am. J. Respir. Crit. Care Med. *187*, 703–714.

De Cecco, M., Ito, T., Petrashen, A.P., Elias, A.E., Skvir, N.J., Criscione, S.W., Caligiana, A., Brocculi, G., Adney, E.M., Boeke, J.D., et al. (2019). L1 drives IFN in senescent cells and promotes age-associated inflammation. Nature *566*, 73–78.

Demaria, M., Ohtani, N., Youssef, S.A., Rodier, F., Toussaint, W., Mitchell, J.R., Laberge, R.M., Vijg, J., Van Steeg, H., Dollé, M.E., et al. (2014). An essential role for senescent cells in optimal wound healing through secretion of PDGF-AA. Dev. Cell *31*, 722–733.

Demaria, M., O'Leary, M.N., Chang, J., Shao, L., Liu, S., Alimirah, F., Koenig, K., Le, C., Mitin, N., Deal, A.M., et al. (2017). Cellular senescence promotes adverse effects of chemotherapy and cancer relapse. Cancer Discov *7*, 165–176.

Dennis, E.A., and Norris, P.C. (2015). Eicosanoid storm in infection and inflammation. Nat. Rev. Immunol. *15*, 511–523.

Dimri, G.P., Lee, X., Basile, G., Acosta, M., Scott, G., Roskelley, C., Medrano, E.E., Linskens, M., Rubelj, I., and Pereira-Smith, O. (1995). A biomarker that identifies senescent human cells in culture and in aging skin in vivo. Proc. Natl. Acad. Sci. USA *92*, 9363–9367.

Flor, A.C., Wolfgeher, D., Wu, D., and Kron, S.J. (2017). A signature of enhanced lipid metabolism, lipid peroxidation and aldehyde stress in therapy-induced senescence. Cell Death Discov *3*, 17075.

Folch, J., Ascoli, I., Lees, M., Meath, J.A., and LeBARON, N. (1951). Preparation of lipide extracts from brain tissue. J. Biol. Chem. *191*, 833–841.

Forman, B.M., Tontonoz, P., Chen, J., Brun, R.P., Spiegelman, B.M., and Evans, R.M. (1995). 15-deoxy-delta 12, 14-prostaglandin J2 is a ligand for the adipocyte determination factor PPAR gamma. Cell *83*, 803–812.

Freund, A., Patil, C.K., and Campisi, J. (2011). P38MAPK is a novel DNA damage response-independent regulator of the senescence-associated secretory phenotype. EMBO J *30*, 1536–1548.

Funk, C.D. (2001). Prostaglandins and leukotrienes: advances in eicosanoid biology. Science *294*, 1871–1875.

Gan, Q., Huang, J., Zhou, R., Niu, J., Zhu, X., Wang, J., Zhang, Z., and Tong, T. (2008). PPAR{gamma} accelerates cellular senescence by inducing p16INK4 {alpha} expression in human diploid fibroblasts. J. Cell Sci. *121*, 2235–2245.

Gibb, W. (1998). The role of prostaglandins in human parturition. Ann. Med. *30*, 235–241.

Giles, H., Leff, P., Bolofo, M.L., Kelly, M.G., and Robertson, A.D. (1989). The classification of prostaglandin DP-receptors in platelets and vasculature using BW A868C, a novel, selective and potent competitive antagonist. Br. J. Pharmacol. *96*, 291–300.

Han, J.H., Roh, M.S., Park, C.H., Park, K.C., Cho, K.H., Kim, K.H., Eun, H.C., and Chung, J.H. (2004). Selective COX-2 inhibitor, NS-398, inhibits the replicative senescence of cultured dermal fibroblasts. Mech. Ageing Dev. *125*, 359–366.

Harkewicz, R., Fahy, E., Andreyev, A., and Dennis, E.A. (2007). Arachidonate-derived dihomoprostaglandin production observed in endotoxin-stimulated macrophage-like cells. J. Biol. Chem. *282*, 2899–2910.

Hata, A.N., and Breyer, R.M. (2004). Pharmacology and signaling of prostaglandin receptors: multiple roles in inflammation and immune modulation. Pharmacol. Ther. *103*, 147–166.

Hernandez-Segura, A., de Jong, T.V., Melov, S., Guryev, V., Campisi, J., and Demaria, M. (2017). Unmasking transcriptional heterogeneity in senescent cells. Curr. Biol. *27*, 2652–2660.e4.

Hickson, L.J., Langhi Prata, L.G.P., Bobart, S.A., Evans, T.K., Giorgadze, N., Hashmi, S.K., Herrmann, S.M., Jensen, M.D., Jia, Q., Jordan, K.L., et al. (2019). Senolytics decrease senescent cells in humans: preliminary report from a clinical trial of dasatinib plus quercetin in individuals with diabetic kidney disease. EBioMedicine *47*, 446–456.

Hirai, H., Tanaka, K., Yoshie, O., Ogawa, K., Kenmotsu, K., Takamori, Y., Ichimasa, M., Sugamura, K., Nakamura, M., Takano, S., and Ngata, K. (2001). Prostaglandin D2 selectively induces chemotaxis in T helper type 2 cells, eosinophils, and basophils via seven-transmembrane receptor CRTH2. J. Exp. Med. *193*, 255–261.

Hirata, M., Kakizuka, A., Aizawa, M., Ushikubi, F., and Narumiya, S. (1994). Molecular characterization of a mouse prostaglandin D receptor and functional expression of the cloned gene. Proc. Natl. Acad. Sci. USA *91*, 11192–11196.

Jump, D.B. (2009). Mammalian fatty acid elongases. Methods Mol. Biol. *579*, 375–389.

Justice, J.N., Nambiar, A.M., Tchkonia, T., LeBrasseur, N.K., Pascual, R., Hashmi, S.K., Prata, L., Masternak, M.M., Kritchevsky, S.B., Musi, N., and Kirkland, J.L. (2019). Senolytics in idiopathic pulmonary fibrosis: results from a first-in-human, open-label, pilot study. EBiomedicine *40*, 554–563.

Kabir, T.D., Leigh, R.J., Tasena, H., Mellone, M., Coletta, R.D., Parkinson, E.K., Prime, S.S., Thomas, G.J., Paterson, I.C., Zhou, D., et al. (2016). A miR-335/COX-2/PTEN axis regulates the secretory phenotype of senescent cancer-associated fibroblasts. Aging (Albany, NY) *8*, 1608–1635.

Kim, J., Vaish, V., Feng, M., Field, K., Chatzistamou, I., and Shim, M. (2016). Transgenic expression of cyclooxygenase-2 (COX2) causes premature aging phenotypes in mice. Aging (Albany, NY) *8*, 2392–2406.

Kliewer, S.A., Lenhard, J.M., Willson, T.M., Patel, I., Morris, D.C., and Lehmann, J.M. (1995). A prostaglandin J2 metabolite binds peroxisome proliferator-activated receptor gamma and promotes adipocyte differentiation. Cell *83*, 813–819.

Kuilman, T., Michaloglou, C., Mooi, W.J., and Peeper, D.S. (2010). The essence of senescence. Genes Dev *24*, 2463–2479.

Laberge, R.M., Zhou, L., Sarantos, M.R., Rodier, F., Freund, A., de Keizer, P.L., Liu, S., Demaria, M., Cong, Y.S., Kapahi, P., et al. (2012). Glucocorticoids suppress selected components of the senescence-associated secretory phenotype. Aging Cell *11*, 569–578.

Lee, J.W., Mok, H.J., Lee, D.Y., Park, S.C., Ban, M.S., Choi, J., Park, C.G., Ahn, Y.S., Kim, K.P., and Kim, H.D. (2016). UPLC-MS/MS-based profiling of eicosanoids in RAW264.7 cells treated with lipopolysaccharide. Int. J. Mol. Sci. *17*, 508.

Martien, S., Pluquet, O., Vercamer, C., Malaquin, N., Martin, N., Gosselin, K., Pourtier, A., and Abbadie, C. (2013). Cellular senescence involves an intracrine prostaglandin E2 pathway in human fibroblasts. Biochim. Biophys. Acta *1831*, 1217–1227.

Menon, R., Behnia, F., Polettini, J., Saade, G.R., Campisi, J., and Velarde, M. (2016). Placental membrane aging and HMGB1 signaling associated with human parturition. Aging (Albany, NY) *8*, 216–230.

Monneret, G., Li, H., Vasilescu, J., Rokach, J., and Powell, W.S. (2002). 15-Deoxy-delta 12,14-prostaglandins D2 and J2 are potent activators of human eosinophils. J. Immunol. *168*, 3563–3569.

Montagut, C., Sharma, S.V., Shioda, T., McDermott, U., Ulman, M., Ulkus, L.E., Dias-Santagata, D., Stubbs, H., Lee, D.Y., Singh, A., et al. (2008). Elevated CRAF as a potential mechanism of acquired resistance to BRAF inhibition in melanoma. Cancer Res *68*, 4853–4861.

Nomura, T., Lu, R., Pucci, M.L., and Schuster, V.L. (2004). The two-step model of prostaglandin signal termination: in vitro reconstitution with the prostaglandin transporter and prostaglandin 15 dehydrogenase. Mol. Pharmacol. *65*, 973–978.

Ohno, Y., Suto, S., Yamanaka, M., Mizutani, Y., Mitsutake, S., Igarashi, Y., Sassa, T., and Kihara, A. (2010). ELOVL1 production of C24 acyl-CoAs is linked to C24 sphingolipid synthesis. Proc. Natl. Acad. Sci. USA *107*, 18439–18444.

Oliva, J.L., Pérez-Sala, D., Castrillo, A., Martínez, N., Cañada, F.J., Boscá, L., and Rojas, J.M. (2003). The cyclopentenone 15-deoxy-delta 12,14-prostaglandin J2 binds to and activates H-Ras. Proc. Natl. Acad. Sci. USA *100*, 4772–4777.

Perretti, M., and D'Acquisto, F. (2009). Annexin A1 and glucocorticoids as effectors of the resolution of inflammation. Nat. Rev. Immunol. *9*, 62–70.

Pettipher, R., Vinall, S.L., Xue, L., Speight, G., Townsend, E.R., Gazi, L., Whelan, C.J., Armer, R.E., Payton, M.A., and Hunter, M.G. (2012). Pharmacologic profile of OC000459, a potent, selective, and orally active D prostanoid receptor 2 antagonist that inhibits mast cell-dependent activation of T helper 2 lymphocytes and eosinophils. J. Pharmacol. Exp. Ther. *340*, 473–482.

Quijano, C., Cao, L., Fergusson, M.M., Romero, H., Liu, J., Gutkind, S., Rovira, I.I., Mohney, R.P., Karoly, E.D., and Finkel, T. (2012). Oncogene-induced senescence results in marked metabolic and bioenergetic alterations. Cell Cycle *11*, 1383–1392.

Renedo, M., Gayarre, J., García-Domínguez, C.A., Pérez-Rodríguez, A., Prieto, A., Cañada, F.J., Rojas, J.M., and Pérez-Sala, D. (2007). Modification and activation of Ras proteins by electrophilic prostanoids with different structure are site-selective. Biochemistry *46*, 6607–6616.

Ricciotti, E., and FitzGerald, G.A. (2011). Prostaglandins and inflammation. Arterioscler. Thromb. Vasc. Biol. *31*, 986–1000.

Rosner, B.A., and Cristofalo, V.J. (1979). Hydrocortisone: a specific modulator of in vitro cell proliferation and aging. Mech. Ageing Dev. *9*, 485–496.

Serrano, M., Lin, A.W., McCurrach, M.E., Beach, D., and Lowe, S.W. (1997). Oncogenic ras provokes premature cell senescence associated with accumulation of p53 and p16INK4a. Cell *88*, 593–602.

Soberman, R.J., and Christmas, P. (2003). The organization and consequences of eicosanoid signaling. J. Clin. Invest. *111*, 1107–1113.

Sprecher, H., VanRollins, M., Sun, F., Wyche, A., and Needleman, P. (1982). Dihomo-prostaglandins and -thromboxane. A prostaglandin family from adrenic acid that may be preferentially synthesized in the kidney. J. Biol. Chem. *257*, 3912–3918.

Strong, R., Miller, R.A., Astle, C.M., Floyd, R.A., Flurkey, K., Hensley, K.L., Javors, M.A., Leeuwenburgh, C., Nelson, J.F., Ongini, E., et al. (2008). Nordihydroguaiaretic acid and aspirin increase lifespan of genetically heterogeneous male mice. Aging Cell *7*, 641–650.

Sun, P., Yoshizuka, N., New, L., Moser, B.A., Li, Y., Liao, R., Xie, C., Chen, J., Deng, Q., Yamout, M., et al. (2007). PRAK is essential for ras-induced senescence and tumor suppression. Cell *128*, 295–308.

Town, M.H., Casals-Stenzel, J., and Schillinger, E. (1983). Pharmacological and cardiovascular properties of a hydantoin derivative, BW 245 C, with high affinity and selectivity for PGD2 receptors. Prostaglandins *25*, 13–28.

Wall, S.B., Oh, J.Y., Mitchell, L., Laube, A.H., Campbell, S.L., Renfrow, M.B., and Landar, A. (2015). Rac1 modification by an electrophilic 15-deoxy Δ(12,14)-prostaglandin J2 analog. Redox Biol *4*, 346–354.

Wiley, C.D., and Campisi, J. (2016). From ancient pathways to aging cells-connecting metabolism and cellular senescence. Cell Metab *23*, 1013–1021.

Wiley, C.D., Velarde, M.C., Lecot, P., Liu, S., Sarnoski, E.A., Freund, A., Shirakawa, K., Lim, H.W., Davis, S.S., Ramanathan, A., et al. (2016). Mitochondrial dysfunction induces senescence with a distinct secretory phenotype. Cell Metab *23*, 303–314.

Wiley, C.D., Schaum, N., Alimirah, F., Lopez-Dominguez, J.A., Orjalo, A.V., Scott, G., Desprez, P.Y., Benz, C., Davalos, A.R., and Campisi, J. (2018). Small-molecule MDM2 antagonists attenuate the senescence-associated secretory phenotype. Sci. Rep. *8*, 2410.

Wiley, C.D., Brumwell, A.N., Davis, S.S., Jackson, J.R., Valdovinos, A., Calhoun, C., Alimirah, F., Castellanos, C.A., Ruan, R., Wei, Y., et al. (2019a). Secretion of leukotrienes by senescent lung fibroblasts promotes pulmonary fibrosis. JCI Insight *4*, e130056.

Wiley, C.D., Liu, S., Limbad, C., Zawadzka, A.M., Beck, J., Demaria, M., Artwood, R., Alimirah, F., Lopez-Dominguez, J.A., Kuehnemann, C., et al. (2019b). SILAC analysis reveals increased secretion of hemostasis-related factors by senescent cells. Cell Rep *28*, 3329–3337.e5.

Yang, H.H., Kim, C., Jung, B., Kim, K.S., and Kim, J.R. (2011). Involvement of IGF binding protein 5 in prostaglandin E(2)-induced cellular senescence in human fibroblasts. Biogerontology *12*, 239–252.

Yoshizuka, N., Chen, R.M., Xu, Z., Liao, R., Hong, L., Hu, W.Y., Yu, G., Han, J., Chen, L., and Sun, P. (2012). A novel function of p38-regulated/activated kinase in endothelial cell migration and tumor angiogenesis. Mol. Cell. Biol. *32*, 606–618.

Zdanov, S., Bernard, D., Debacq-Chainiaux, F., Martien, S., Gosselin, K., Vercamer, C., Chelli, F., Toussaint, O., and Abbadie, C. (2007). Normal or stress-induced fibroblast senescence involves COX-2 activity. Exp. Cell Res. *313*, 3046–3056.

STAR★METHODS

KEY RESOURCES TABLE

REAGENT or RESOURCE	SOURCE	IDENTIFIER
Antibodies		
Phospho-PRAK-T182	Peiqing Sun - Wake Forest Univeristy	N/A
Phospho-p53 (Ser37) Antibody	Cell Signaling Technology	#9289
p21 Waf1/Cip1 (12D1) Rabbit mAb	Cell Signaling Technology	#2947
Phospho-p44/42 MAPK (Erk1/2) (Thr202/ Tyr204) Antibody	Cell Signaling Technology	#9101
p44/42 MAPK (Erk1/2) Antibody	Cell Signaling Technology	#9102
p38 MAPK Antibody	Cell Signaling Technology	#9212
Anti-Lamin B1 antibody	Abcam	ab16048
Anti-HMGB1 antibody	Abcam	ab18256
Monoclonal Anti-β-Actin antibody	Sigma	A2228
p53 Antibody (DO-1)	Santa Cruz Biotechnology	sc-126
Bacterial and virus strains		
shGFP lentivirus	Campisi Lab	N/A
shP53 lentivirus	Campisi Lab	N/A
shPTGDS lentivirus	Sigma-Aldrich	SHCLNV-NM_000954
Chemicals, peptides, and recombinant proteins		
NS-398	Cayman Chemical Company	70590
CAY-10404	Cayman Chemical Company	70210
Ciglitazone	Cayman Chemical Company	71730
Troglitazone	Cayman Chemical Company	71750
Staurosporine	Cayman Chemical Company	81590
Recombinant Human TRAIL protein	Abcam	ab78818
Arachidonic Acid-d_{11}	Cayman Chemical Company	10006758
Prostaglandin A_2	Cayman Chemical Company	10210
Prostaglandin D_2	Cayman Chemical Company	12010
Prostaglandin E_2	Cayman Chemical Company	14010
Prostaglandin $F_{2\alpha}$	Cayman Chemical Company	16010
Prostaglandin J_2	Cayman Chemical Company	18500
15-deoxy-$\Delta^{12,14}$-Prostaglandin J_2	Cayman Chemical Company	18570
1a,1b-dihomo-15-deoxy-$\Delta^{12,14}$-Prostaglandin J_2	Jubilant Chemsys	P1171
13,14-dihydro-15-keto Prostaglandin D_2	Cayman Chemical Company	12610
BW A868C	Cayman Chemical Company	12060
OC000459	Cayman Chemical Company	12027
BW 245C	Cayman Chemical Company	12050
Hydrocortisone	Cayman Chemical Company	20739
Acetic Acid, glacial	VWR	VW0125-3
Acetonitrile	VWR/BDH	BDH83639.400
Ammonium acetate	Sigma Aldrich	73594-25G-F
LCMS Water	Honeywell Burdick & Jackson	LC365-4
Methanol	Honeywell Burdick & Jackson	LC230-4
Chloroform	JT Baker	9175-2
Critical commercial assays		
Baculoviral PPAR-gamma reporter assay	Signosis	BT-0014
Senescence Detection Kit	BioVision	K320

(*Continued on next page*)

Continued		
REAGENT or RESOURCE	SOURCE	IDENTIFIER
15-deoxy-Δ12,14-PGJ2 ELISA Kit	ENZO	ADI-900-023
Prostaglandin D2-MOX Express ELISA Kit	Cayman Chemical Company	500151
IL-6 AlphaLISA	PerkinElmer	AL223F
Ras Pull-down Activation Assay Biochem Kit	Cytoskeleton	BK008-S
Deposited data		
Lipid Profiling Dataset	National Metabolomics Data Repository (NMDR)	PR001093
Experimental models: Cell lines		
HEPG2	ATCC	HB-8065
IMR-90	ATCC	CCL-186
HUVEC-C	ATCC	CRL-1730
Experimental models: Organisms/strains		
C57BL/6J	The Jackson Laboratory	000664
p16-3MR	Campisi Laboratory	N/A
Teklad global 18% protein	Envigo Teklad	2918
Oligonucleotides		
See Table S2	N/A	N/A
Software and algorithms		
MassHunter	Agilent	N/A
Other		
Kinetex 5μm EVO C18 100Å 150x2.1mm	Phenomenex	00F-4633-AN

RESOURCE AVAILABILITY

Lead contact

Further information and requests for resources and reagents should be directed to and will be fulfilled by the Lead Contact, Judith Campisi (jcampisi@buckinstitute.org).

Material availability

This study did not generate unique reagents. The schematic for synthesis of dihomo-15d-PGJ2 will be provided upon request.

DATA AND CODE AVAILABILITY

Lipid profiling data is available at the NIH Common Fund's National Metabolomics Data Repository (NMDR) website, the Metabolomics Workbench (https://www.metabolomicsworkbench.org), Project ID #: PR001093. See also the Key resources table.

EXPERIMENTAL MODEL AND SUBJECT DETAILS

Cell lines and strains

All cells were purchased from the American Type Culture Collection (ATCC), see Key resources table. IMR-90 human female fetal lung fibroblasts were the primary cell type used in this study, and were used prior to 40 population doublings - other than replicative senescent cells, which were cultured until replicative exhaustion. HEPG2 human adolescent male hepatocellular carcinoma are immortalized, but p53-positive, and therefore no population doublings were recorded. IMR-90 and HEPG2 cells were cultured in Dulbecco's modified eagle medium (DMEM 4.5 g/L glucose, without sodium pyruvate - Gibco) supplemented with 10% FBS and penicillin/streptomycin (Gibco). HUVEC human female umbilical vein endothelial cells were cultured using the ATCC protocol and culture media and assayed within 40 population doublings. Quiescence was induced by replacing culture media with media containing 0.2% FBS for 72 h before analysis. All cells were cultured at 37°C and 3% O_2. All cells were mycoplasma free.

Animals

Animal experiments were conducted using a protocol approved by the Institutional Animal Care and Use Committee of the Buck Institute. Mice were housed in alternating 12:12 hour light/dark cycles at 68-72°F. General animal health rounds were performed daily,

7 days a week by trained Vivarium staff members. Any noted illness or deaths were reported via the Health Surveillance system to the Vivarium Director and/or the Attending Veterinarian (AV). The Buck Vivarium is an SPF barrier facility and routine health screening is done facility-wide to ensure the health of all colonies. Sentinel mice that were exposed to soiled bedding and byproducts from other mice on the same rack were screened quarterly for common murine viruses as directed by the AV. Internal and external parasitology screening was also done on all sentinel mice. For DOXO treatments, 10-16 wk old male p16-3MR transgenic mice on a C57BL/6 background received one intraperitoneal (i.p.) injection of 10 mg/kg of doxorubicin hydrochloride in PBS, and treated 5 d later with GCV or vehicle. GCV was administered via daily i.p. injections for 5 consecutive days at 25 mg/kg in PBS. Control mice were injected with an equal volume of PBS. Mice were euthanized and tissues collected 10 d after DOXO challenge. For aging studies, 8 male and 8 female C57BL/6 mice were aged for 6 or 24 mo, at which point mice were euthanized and tissues collected for analysis. For the biomarker studies, 10 male C57BL/6 mice per cohort with challenged with DOXO as above, and given either vehicle or ABT-263 6 weeks after DOXO challenge. Whole blood was collected by cardiac puncture into EDTA-tubes (lavender caps – BD Biosciences) and spun at 2000g for 5 minutes. For urine collection, mice were placed in plastic containers prior to euthanasia.

METHOD DETAILS

Gene expression

RNA was extracted from cells or tissues using commercially available kits (Isolate II - Bioline for cells; Direct-zol - Zymo for tissues) according to the manufacturer's instructions. cDNA synthesis was performed using a High Capacity cDNA Reverse Transcription Kit (Thermo Fisher) according to the manufacturer's instructions. Quantitative PCR was performed on a LightCycler 480 II (Roche) using primers and probes designed for the Universal Probe Library. Primers and probes used for human transcripts are listed in Table S2.

Induction of senescence

Senescence SEN(IR) was induced by either 5 or 10 Gy ionizing-irradiation (IR). Non-senescent controls (proliferating or quiescent) were placed in the irradiator for an identical period of time but without irradiation. Oncogene-induced senescence was induced using lentiviral-mediated overexpression of $HRAS^{V12}$, as described (Wiley et al., 2016), and the lentiviral backbone (Vector) served as a control. MiDAS was induced by depleting mitochondrial DNA in the presence of 100 ng/mL ethidium bromide, 100 ug/mL sodium pyruvate, and 50 ug/mL uridine for 2 months, followed by removal of pyruvate, as described (Wiley et al., 2016).

Generation of conditioned media

Conditioned media (CM) were generated by culturing cells in appropriate serum-free media supplemented with penicillin/streptomycin for 24 h before harvest, followed by clarification by centrifugation. Cells were then trypsinized and counted. All quantitative assays (e.g. ELISAs) from CM were normalized to cell number.

Induction of apoptosis or senolysis

Non-senescent or SEN(IR) cells were cultured in the presence of 10 μM ABT-263 for 24 h. Non-senescent IMR-90 fibroblasts were treated with either 1 μM staurosporine (Cayman) or 100 ng/mL recombinant TRAIL (Abcam) for 24 h before collection. Media were centrifuged twice at 5000xg for 15 minus at 4°C for clearing of apoptotic bodies and stored at -80°C until analysis.

Senescence-associated beta-galactosidase

SA-Bgal activity was detected as described (Dimri et al., 1995) using a commercial kit (Biovision).

Colony forming assay

Ras-transduced senescent cells were plated at a density of 1000/well and cultured in the presence of growth media containing either DMSO, CAY-10404, or NS-398 for 7 days. Cells were washed in PBS, fixed in 95% methanol, and incubated for 30 min in 0.2% crystal violet in 2% methanol. Crystal violet was removed and wells were washed in tap water until the solution ran clear, and allowed to dry.

RAS activation assay

Active RAS (RAS:GTP) was immunoprecipitated from culture lysates using a commercial kit (Cytoskeleton) following the manufacturer's instructions. Precipitates were analyzed by immunoblot.

Immunoblots

Cells were lysed in 5% SDS in 10 mM Tris, pH 7.4, and protein content determined by BCA assay. 20 μg protein was separated by electrophoresis and transferred to PVDF membranes. Membranes were blocked in TBST + 5% BSA, incubated overnight with primary antibody, washed in TBST, incubated with HRP-conjugated secondary antibody for 30 min, and visualized by chemiluminescence – combined with either film or on a BioRAD Hood II Gel Doc universal imager. Antibodies to phosphorylated p53-S37, p21, phospho-ERK1/2, total ERK1/2 and total p38MAPK were from Cell Signaling. Antibodies against LMNB1, HMGB1, and actin were from Abcam, anti-phospho-p38 was from PhosphoSolutions, and anti-PRAK was from Novus. Anti-phospho-PRAK-T182 was a kind gift from Peiqing Sun, and was described in Yoshizuka et al. (2012). Anti-RAS was provided in the kit provided by Cytoskeleton (above).

IL-6 ELISA

$3x10^4$ cells in 12-well plates were treated as indicated, and cultured in 0.5–1 ml serum-free DMEM for 24 hr. CM were collected and clarified at 2,000x g for 10 min. Supernatants were transferred to a tube; cells were trypsinized and counted. CM (2.5 μl) were analyzed by bead-based ELISAs (AlphaLISA, Perkin-Elmer) as instructed by the manufacturer and normalized to cell number.

PGD2-MOX ELISA

CM were isolated as for IL-6 ELISA (above), and analyzed according the manufacturer's instructions (Cayman Chemical), and quantified as pg/cell.

15d-PGJ2 ELISA

$1x10^5$ cells in 6-well plates were treated as indicated for 10 days, and then cultured in 1 ml of serum-free medium plus DMEM or ABT-263 for 24 h. CM were then clarified by centrifugation at 2,500x g for 10 min. 15d-PGJ2 ELISA was from Enzo Life Sciences, and was performed according to the manufacturer's instructions. Cell culture supernatant was analyzed directly, and all numbers were normalized to cell number. For in vivo fluids, 250 μL of blood plasma or 50 μL of urine were extracted as in Liquid-liquid extraction (LLE - below) with the following modification – dehydrated lipid samples were resuspended in 250 μL of assay buffer before analysis.

Reporter assays

Baculoviral PPARγ reporter constructs (Signosis) were transduced into proliferating cells. Following treatment, cells were lysed using Passive Lysis Buffer (Promega) and analyzed for luciferase activity using a commercial kit (Promega) and Perkin-Elmer Victor X3 luminometer.

Chemicals and standards

Ammonium acetate was from Sigma Aldrich (St. Louis, MO). HPLC-grade solvents acetonitrile and methanol were from Fisher Scientific (Pittsburgh, PA, USA) and VWR (Radnor, PA, USA). Deionized water was generated in-house. PGA2, PGD2, PGE2, PGF2α, PGJ2, 15d-PGJ2, 15d-PGJ2-d4, NS-398, CAY-10404, ciglitazone, troglitazone and staurosporine were from Cayman Chemical. ABT-263 was from Apex Biotechnology. The dihomo-15d-PGJ2 standard was synthesized by Jubilant Chemsys (Bangalore, India). TRAIL was from Abcam.

Liquid-liquid extraction (LLE) of lipids

Lipid extraction was performed as reported (Bligh and Dyer, 1959; Folch et al., 1951) with some modifications. Cells were rinsed with PBS and quenched using 1mL 50% methanol; 2 μg/mL 13C1-leucine and 5 ng/mL hexanesulfonic acid were added as internal standards. 2 mL of chloroform with 1 μg/mL heptadecanoic acid was added to each sample and mixed for 10 min at 4° C. Samples were centrifuged at 4,000g for 15 min at 4° C to separate aqueous and organic layers. After centrifugation, 700 μL of the aqueous layer and 1.5 mL of the organic layer were recovered and concentrated by speedvac and N2, respectively. Both aqueous and organic fractions were reconstituted in 100μL 50% methanol and chloroform prior to liquid-chromatography mass spectrometry (LC-MS) analysis.

Solid phase extraction (SPE) of lipids

Lipid extraction was performed based as reported (Harkewicz et al., 2007) with some modifications. Cells were rinsed with PBS and quenched in 1 mL methanol with 2 μg/mL 13C1-leucine, 1μg/mL heptadecanoic acid, and 5 ng/mL hexanesulfonic acid added as internal standards. 1 mL PBS was added to each sample and mixed for 10 min. Samples were centrifuged at 4,000g for 15 min at 4° C. Following centrifugation, oxylipins were separated on Phenomenex Strata-X polymeric sorbent columns connected to a vacuum manifold. Columns were pre-washed with 2 mL methanol followed by 2 mL water. Samples were loaded onto columns, washed with 2 mL 90:10 water:methanol, then eluted with 1mL 100% methanol. Extracts were concentrated by speedvac and reconstituted in 100μL 100% methanol prior to LC-MS analysis.

High-pressure liquid chromatography quadrupole-time-of-flight mass spectrometry (HPLC-QTOF-MS)

LC-MS analyses were performed on a Agilent 6520 QTOF mass spectrometer coupled to a Agilent 1260 Infinity liquid chromatography system consisting of the following modules: u-degasser (G1322A), binary pump (G1312B), thermostated column compartment (G1330B), and HiPALS auto sampler (G1367E). Chromatographic separation of cellular extracts was performed on a Phenomenex Luna NH2 (2.0mm x 150mm, 3.0μM) column. The mobile phase included A:20mM ammonium acetate and 5% acetonitrile, pH9.5 and B:acetonitrile. The gradient is as follows: 0 to 20min, 95-10%B, 25-30min 10%B, and 30.1-35min 95%B. LC conditions included an auto sampler temperature of 4° C, injection volume of 10μL and solvent flow-rate of 0.3mL/min. Analyses were performed using the following ionization parameters: gas temperature (TEM) 350°C; drying gas, 9L/min; Vcap, 2500V; nebulizer, 35psig; fragmentor, 125V; and skimmer, 65V. MS1 acquisition was operated in the negative ion scanning mode for a mass range of 50-1000 m/z.

LC-MS data was acquired and analyzed using Agilent MassHunter Workstation (B.05.00), Agilent MassHunter Qualitative Analysis Software (B.08.00), Mass Profiler Professional (B.12.0), and Microsoft Excel 2007 (Redmond, WA, USA). Peak areas were assigned using Agilent MassHunter Qualitative Analysis Software in combination with the Find by Formula (FBF) algorithm. Peak areas were normalized to total protein or cell number.

High-pressure liquid chromatography quadropole ion trap mass spectrometry (HPLC-QTRAP-MS)

HPLC was performed using a Shimadzu UFLC prominence system fitted with following modules: CBM-20A (Communication bus module), DGU-A_3(degasser), two LC-20AD (liquid chromatography, binary pump), SIL-20AC HT (auto sampler) and connected to a Phenomenex Luna NH_2 (2.0mm x 150mm, 3.0μM) column. The solvent system was A=20mM ammonium acetate pH 9.5 with 5% acetonitrile and B=acetonitrile. The starting gradient conditions were 95% B at a flow rate of 0.3mL/min. The following gradient program was used: 0 to 20min, 95-10%B, 25-30min 10%B, and 30.1-35min 95%B. Samples were kept at +4°C, and the injection volume was 10μL.

Mass spectrometric analysis was conducted using negative ion electrospray ionization in the multiple reaction monitoring mode (MRM) on an AbSciex 4000 QTRAP (Foster City, CA, USA) mass spectrometer fitted with a TurboV ion source. The ionization parameters were set as follows: curtain gas (CAD); 20psi; collision gas: medium; ion spray voltage (IS): -4500V; Temperature (TEM): 550°C; Ion source Gas 1 (GS1); 60psi; and Ion source Gas 2 (GS2): 50psi. The compound parameters were established using appropriate standards. The compound parameters were set as follows: entrance potential (EP): -10.0V; and collision cell exit potential (CXP): -5V. ABSciex Analyst v1.6.1 was used for all data acquisition and an in-depth analysis of the HPLC-MS data, specifically for calculating the peak areas for the identified features from cellular extracts. Peak areas were normalized to total protein.

Reverse-phase LC-MS method for detection of 15d-PGJ2

The LC-MS analysis was performed using Agilent 6520 accurate mass quadruple time of flight (Q-ToF) mass spectrometer coupled with Agilent 1260 Infinity Pump (Agilent Technologies, Santa Clara, CA). Ionization was performed in negative mode. Nitrogen was used as a desolvation and collision gas. The separation was carried out using Kinetex EVO C18 100Å 150x2.1, 5 micron (serial #H15173269) from Phenomenex. The autosampler was set at 5°C. The solvent system was composed of Solvent A- 0.1% acetic acid in 95:5 (water: ACN) containing 10 mM ammonium acetate and Solvent B- 0.1% acetic acid in 95:5 (ACN: water) containing 10 mM ammonium acetate. The flow rate was maintained at 0.3 mL/min, and the initial solvent conditions started with 5% solvent B. At 2 min, the percentage of B was increased to 70% B over 14 min, followed by further increase of % B to 95% for 10 mins. At 24 mins % B was maintained at 95% B for 5 mins and then reduced to 5%B and maintained at 5% B for 5 mins. The run time was 35 mins. Drying gas flow and temperature was set at 9.0 L/min and 350°C, respectively and nebulizer gas pressure was set at 35 psig. The applied capillary voltage was 3000 V. Full scan spectra was acquired from 100-1000 m/z. The instrument was operated with Agilent MassHunter Work station LC/MS Data Acquisition version 05.01, and chromatograms were processed with MassHunter Workstation qualitative software version B.08.00.

Quantitation of intracellular dihomo-15d-PGJ2 concentration

A standard curve was generated using 100, 50, 25, and 10 nM dihomo-15d-PGJ2, and peak areas were quantified by mass spectrometry. Based upon an average measured concentration of 69 nM in 1 mL of cell lysate representing 5 x 10^6 senescent cells, and assuming an average volume of 7.5 pL per senescent cell, we estimated a mean intracellular concentration of 1.8 μM by mass spectrometry, or 5.8 μM by ELISA.

QUANTIFICATION AND STATISTICAL ANALYSIS

Data representation and statistical analysis

All data are presented as means ± SEM, with the exception of box plots, which follow the standard median/quartile structure. All culture datasets represent means of at least 3 experiments, and mouse datasets reflect a minimum of 6 mice. Comparisons between groups were performed using a 2-tailed Student's t test, 1- or 2-way ANOVA, as appropriate. No methods were used to determine whether the data met the assumptions of the statistical approaches. Heat maps use $p < 0.05$ for all entities. Significance is indicated by *$p < 0.05$, **$p < 0.01$, and ***$p < 0.001$. Statistical parameters can be found in Figure legends.